AD-A016 536

HYDRODYNAMIC STABILITY AND TRANSITION TO
TURBULENCE IN THE HYPERSONIC BOUNDARY LAYER
OVER A SHARP CONE

Anthony Demetriades

Aeronutronic Ford Corporation

AFOSR - TR - 75 - 1435

ADA016536

Aeronutronic Publication No.

AFOSR TR_____

HYDRODYNAMIC STABILITY AND TRANSITION

TO TURBULENCE IN THE HYPERSONIC BOUNDARY LAYER

OVER A SHARP CONE

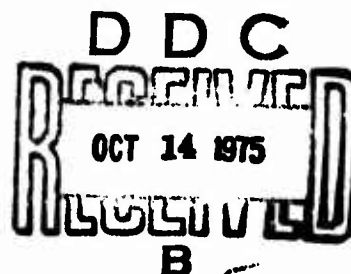Contract USAF/OSR F44620-75-C-0016

by

A. Demetriades

Prepared for

Department of the Air Force
Office of Scientific Research
Washington, D.C.

15 July 1975
Aeronutronic Division
Aeronutronic Ford Corporation
Newport Beach, Calif.

Approved for public release;
distribution unlimited

Aeronutronic *Ford*

Aeronutronic Ford Corporation
Aeronutronic Division
Newport Beach, California

Qualified requestors may obtain additional copies from the Defense
Documentation Center, all others should apply to the National Technical
Information Service.

Conditions of Reproduction

Reproduction, translation, publication, use and disposal in whole or in
part by or for the United States Government is permitted.

REPORT DOCUMENTATION PAGE		READ INSTRUCTIONS BEFORE COMPLETING FORM
1. REPORT NUMBER AFOSR - TR - 75 - 1 1 7	2. GOVT ACCESSION NO.	3. RECIPIENT'S CATALOG NUMBER
4. TITLE *(and Subtitle)* HYDRODYNAMIC STABILITY AND TRANSITION TO TURBULENCE IN THE HYPERSONIC BOUNDARY LAYER OVER A SHARP CONE		5. TYPE OF REPORT & PERIOD COVERED INTERIM 1 Oct 1974 - 30 June 1975
		6. PERFORMING ORG. REPORT NUMBER
7. AUTHOR(s) ANTHONY DEMETRIADES		8. CONTRACT OR GRANT NUMBER(s) F44620-75-C-0016
9. PERFORMING ORGANIZATION NAME AND ADDRESS AERONUTRONIC FORD AERONUTRONIC FORD CORPORATION, AERONUTRONIC DIVISION NEWPORT BEACH, CALIFORNIA 92663		10. PROGRAM ELEMENT, PROJECT, TASK AREA & WORK UNIT NUMBERS 681307 9781-03 61102F
11. CONTROLLING OFFICE NAME AND ADDRESS AIR FORCE OFFICE OF SCIENTIFIC RESEARCH/NA 1400 WILSON BOULEVARD ARLINGTON, VIRGINIA 22209		12. REPORT DATE July 1975
		13. NUMBER OF PAGES 4F 4 9
14. MONITORING AGENCY NAME & ADDRESS*(if different from Controlling Office)*		15. SECURITY CLASS. *(of this report)* UNCLASSIFIED
		15a. DECLASSIFICATION DOWNGRADING SCHEDULE

16. DISTRIBUTION STATEMENT *(of this Report)*

Approved for public release; distribution unlimited.

17. DISTRIBUTION STATEMENT *(of the abstract entered in Block 20, if different from Report)*

18. SUPPLEMENTARY NOTES

19. KEY WORDS *(Continue on reverse side if necessary and identify by block number)*

HYPERSONIC FLOW	TRANSITION
BOUNDARY LAYER	TURBULENCE
VISCOUS FLOW	LAMINAR FLOW
CONE	
STABILITY	

20. ABSTRACT *(Continue on reverse side if necessary and identify by block number)*
Periodic oscillations have been observed in the laminar boundary layer of a sharp tipped, 5-degree adiabatic cone immersed in a stream of Mach no. 8. These oscillations have been photographed with a spark shadowgraph system and probed with a hot-wire anemometer. The waves possess higher harmonics and are most intense near the edge of the boundary layer, although they remain finite for some distance beyond the edge. They consist mostly of two-dimensional structures in the fluid density, travel nearly with the stream velocity and amplify selectively so that their wavelength remains nearly twice the boundary layer

DD FORM 1473 EDITION OF 1 NOV 65 IS OBSOLETE

thickness as the latter grows. Such evidence indicates that the waves are due to a hydrodynamic instability of the Tollmien-Schlichting type, active in the range $Re_x > 2 \times 10^6$. At about $Re_x = 4 \times 10^6$ the oscillation undergoes Fourier dispersion ("line broadening") which results in a fully random spectrum, characteristic of turbulence, by $Re_x = 5.5 \times 10^6$. This implies that transition is caused by break-up of these waves, as also corroborated by meanflow profiles, surface data and shadowgrams taken simultaneously. Comparison shows that transition is first signaled by the appearance of these waves, much earlier than detected by ordinary sensors. Surface sensors seem to give a false elongation of the transition zone, perhaps because of the thermal diffusion on the wall.

ABSTRACT

Periodic oscillations have been observed in the laminar boundary layer of a
sharp-tipped, 5-degree adiabatic cone immersed in a stream of Mach number 8.
These oscillations have been photographed with a spark shadowgraph system
and probed with a hot-wire anemometer. The waves possess higher harmonics
and are most intense near the edge of the boundary layer, although they re-
main finite for some distance beyond the edge. They consist mostly of two-
dimensional structures in the fluid density, travel nearly with the stream
velocity and amplify selectively so that their wavelength remains nearly
twice the boundary layer thickness as the latter grows. Such evidence in-
dicates that the waves are due to a hydrodynamic instability of the Tollmien-
Schlichting type, active in the range $Re_x > 2 \times 10^6$. At about $Re_{e_x} = 4 \times 10^6$
the oscillation undergoes Fourier dispersion ("line broadening") which results
in a fully random spectrum, characteristic of turbulence, by $Re_x = 5.5 \times 10^6$.
This implies that transition is caused by break-up of these waves, as also
corroborated by mean-flow profiles, surface data and shadowgrams taken simul-
taneously. Comparison shows that transition is first signaled by the appear-
ance of these waves, much earlier than detected by ordinary sensors. Surface
sensors seem to give a false elongation of the transition zone, perhaps be-
cause of the thermal diffusion on the wall.

MAJOR CONCLUSIONS

1. The intimate connection found between the observed laminar waves and
   transition on the frustum verifies the predicted role of hydrodynamic
   instability in the transition-to-turbulence process.

2. Examination of and measurements from the available tapes should be con-
   tinued and completed.

3. New measurements should be performed to extend the available data to con-
   figurations with surface roughness, cooling and mass addition, utilizing
   the existing hardware, techniques and facilities.

4. Theoretical transition-prediction methods should be directed more intensely
   if not exclusively, to the hydrodynamic stability of the boundary layer.

TABLE OF CONTENTS

LIST OF SYMBOLS

fo : frequency of laminar oscillations

ℓ : wavelength of laminar oscillations

M : Mach number

p : static pressure

P_o : stagnation pressure of wind-tunnel

P_t : pitot pressure

Re' : unit Reynolds number

Re_x : Reynolds number based on x

$Re_{\infty D}$: Reynolds number based on tunnel diameter

St : Stanton number

T_o : stagnation temperature of wind-tunnel

T_t : total temperature (local)

T_w : wall temperature

u : flow velocity

x : distance from cone tip

y : distance from wall (cone surface)

α : angle of attack

γ : ratio of specific heats

δ : boundary-layer thickness

δ^* : boundary-layer displacement thickness

θ : boundary-layer momentum thickness

$\dot{m}$: mass-injection rate at the surface

ρ : density

$(\overline{\ \ })$: mean quantities

$(\ )_e$: at boundary-layer edge

$(\ )_\infty$: in the free-stream

$(\ )'$: root-mean-square wideband fluctuation

iii

LIST OF ILLUSTRATIONS

1. DESCRIPTION OF EXPERIMENT

The data described herein were obtained from magnetic tapes generated in the course of an extensive study of the hypersonic boundary layer on a cone. Reference 1 describes the overall turbulent boundary layer and model surface properties observed in the test matrix, while Reference 2 concentrates on the turbulence properties following transition.

For the sake of completeness, the experiment conditions will be outlined briefly. The tests were done at Wind-Tunnel B of the Arnold Engineering Development Center (AEDC) at Tullahoma, Tennessee, shown on Figure 1. Flow conditions were: Mach number $M_\infty = 8$, Reynolds number $Re'_\infty = 1.7 \times 10^6$ to 2.6×10^6 per foot and total temperature $T_0 = 750°K$ ($1360°R$). The flow was continuous (e.g., 10 hours) and the flow uniformity in the test section very satisfactory (standard deviation of 0.01 in the Mach number). Free-stream turbulence levels were measured as follows: pressure $p'/p_\infty = 4.9$ to 3.7 percent, and temperature fluctuations $T'/T_\infty = 4.5$ to 3 percent (as Re'_∞ increases). These fluctuation levels are consistent with wind-tunnels of the size used, and interferred neither with the transition process nor with the detection of the boundary-layer instabilities.

All data were obtained at nearly adiabatic conditions in the boundary-layer of the heavily instrumented 5-foot long, 5-degree half-angle circular cone with a very sharp nosetip, supplied by the General Electric Company and shown on Figure 2. For certain portions of the experiment, the model was pitched to ± 3 degrees angle of attack, while for others air was uniformly injected through its porous surface at carefully metered rates to simulate various levels of material ablation. Surface pressures, temperatures and heat rates were monitored continuously throughout the experiment. Furthermore, external instrumented rake mounting miniature probes were traversed vertically to the surface at various distances from the tip, to obtain high resolution boundary-layer profiles as shown on Figure 3. A complete spark-shadow photographic file of the flow at each testing condition was also made.

One of the probes used was a sub-miniature hot-wire anemometer coupled to a specifically constructed compensated amplifier, set to measure unsteady signals to beyond 1 MHz - a factor of five higher than the frequency of any observed instability. Just prior to the measurement, each hot-wire was individually calibrated, and at each point in the flow it underwent changes of its bias current necessary for later separation of its signals into flow variables. The probe signals were recorded both on FM (500 kHz) and direct (1.5 MHz) channels of a 1/2 inch tape magnetic recorder, with 5 other channels receiving simultaneous data on the probe position, pitot pressure, etc.

The taped data containing boundary-layer stability information fall into two categories. "High resolution" data were recorded at fixed distances x from the cone tip (x = 19, 29, 39 and 55 inches) and at ten vertical distances from the model surface at each x, usually in increments of about 0.1δ. At each point, moreover, the wire output was recorded for 6 to 7 seconds at 120 kps for each "overheat" (bias current) to enable later "modal analysis"; i.e.,

1

separation into flow variables. These data were taken primarily with 0.00002"
dia. hot-wires which have a superior signal-to-noise ratio; they are ideal
for modal and Fourier analysis of the instabilities and for their spatial
resolution in the vertical (y) direction. They are less suited for amplifi-
cation-rate measurements because of the large separation between x positions.
In the second category, there are "low resolution" data obtained with 0.00005"
dia. wires for P_o = 150 psia at intervals Δx = 2 inches between x^o = 19 and
39 inches (Re_x range from 1.37 x 10^6 to 2.8 x 10^6) and, for P_o = 350, between
x = 19 and 39 inches (Re_x range from 3.2 x 10^6 to 6.5 x 10^6); these span the
entire instability-transition process, from the first appearance of oscilla-
tions to complete turbulence breakdown. In these cases, the hot-wire was
traversed vertically at each x, continuously from $y \simeq 0$ to beyond the layer
edge at nearly constant speed and for a single fixed (high) bias-current
setting. From such data the stream-wise evolution of instabilities and their
spectrum can be determined, if one is content with using the unresolved "raw"
hot-wire signal alone.

2. METHOD OF MAGNETIC TAPE RECORDING

The magnetic tape "library" utilized in this contract was collected as follows:
The hot-wire (HW), total-temperature probe (T_t) and pitot tube (P_t) supplied
signals to the circuits diagrammed in Figure 4. For the "high resolution"
data (see above), the probes were fixed at some distance y above the cone
surface at a length x away from the cone tip. The tape recorder was started
and the hot-wire signals were transmitted to channels 1 (FM) and 4 (direct)
of the recorder through the ADP 1213 amplifier. At the same time the mean
wire voltage was deposited on channel 3 (FM) after voltage-to-frequency con-
version into a pulse train. Similar VFC conversion was used to deposit the
T_t and P_t signals on channels 5 and 7 respectively. A 20 KHz tone signal
was also recorded on channel 2 to mark the record duration (so that, on play-
back, the operator knows when it is permissible to process signals for that
particular x and y). At the end of 10 seconds, the tone was interrupted, the
tape recorder stopped, and the probe rake moved to another position y, where
the process was repeated. When sufficient y points had been probed, the rake
was removed to another distance x behind the nose-tip and the process repeated.

For tape no. 65, which contains the "low resolution" data, the process was
modified slightly, by connecting a voltage source indicating y (i.e. probe
position above the cone surface) to channel 6. The probes were brought (as
closely as possible) to the surface and the tape recorder started. Then the
channel 2 tone was switched "on" and the probe was actuated to move at con-
stant speed away from the surface, through the boundary-layer and into the
free-stream. Shortly after probe exit from the boundary-layer (e.g. $y \cong 2$)
the tone was switched "off" and the probe motion and tape recorder stopped.

3. INSTABILITY OBSERVATIONS IN THE LAMINAR LAYER

The existence and intensity of the laminar waves were first revealed by the
shadow photographs such as Figure 5 taken routinely during the wind-tunnel
tests noted above. The photographs showed that the waves were always present

2

in the laminar boundary-layer; it was common to find a wave train 10-20 wavelengths long upstream of transition. The waves appeared even in the presence of mass injection and angle of attack, and increased in intensity along the flow. Significantly, photographs taken at random over a period of many testing days, showed that (a) transition to turbulence was always preceded by the appearance of the instability, (b) there was no case noted where the waves were not followed by transition.

Typical waveforms obtained with the low-resolution hot-wire anemometer are shown in Figures 6 and 7. It is clear, as will be reiterated below, that the fluctuation magnitude is highest near, and in fact persists considerably beyond, the boundary-layer edge δ as measured from the velocity profile (see Reference 2 for details on computing δ). Using δ and the edge velocity u_e the non-dimensional fluctuation wavelength $\ell/\delta = u_e/f_o\delta$ was found from the center frequency f_o of the fluctuation, using the spectrum plots discussed below. Figure 8 shows that $\ell \simeq 2\delta$ and grows much slower with x than does δ, giving proof that the observed waves are related to the model boundary layer as opposed to the tunnel flow. For surface blowing at $\lambda = 0.0015$, ℓ/δ remained constant with Re_x but its value increased to about 4. In terms of actual frequency these signals occur in the range 40-180 KHz*.

High resolution energy spectra of the hot-wire output are shown on Figure 9. Note the appearance of a "higher harmonic" in these plots. Although not all the taped data have been examined yet in detail, as many as two such harmonics (additional to the main peak) have been discerned so far.

A limited portion of the hot-wire signals such as shown in Figures 5-9 have been separated into local, wideband root-mean-square temperature T'/T and velocity $u'/\bar{u}$ fluctuations. The distribution of these with distance y from the wall are shown typically on Figure 10. The remarkable feature of this result is that, whereas the temperature (density) fluctuations are very large (25 percent) the corresponding velocity fluctuations are miniscule, and in fact show no prominence at all at $y/\delta = 0.97$. This finding is completely consistent with total enthalpy conservation and says that, in contrast with the low-speed case, the flow does not actually oscillate but rather forms a succession of peaks and valleys in its own density. Thus, although the frequency characteristics conform to classical stability theory, the physical character of the oscillation is totally new.

---

*A question has been raised as to how it is possible to "change frequencies" between two x positions. This is explainable by selective amplification, by which each Fourier component continuously amplifies or damps along the flow. In fact this explanation is strong evidence that the observations agree with the linear hydrodynamic stability theory.

4. FREE-STREAM TURBULENCE LEVEL

All transition experiments should include a description of the free-stream turbulence, i.e. the ambient disturbance level. For this test, this level was measured quantitatively as follows:

$$u' \quad \text{(velocity fluctuations)} \quad 6$$
$$T' \quad \text{(temperature fluctuations) } 4.5\%$$
$$p' \quad \text{(pressure fluctuations)} \quad 4.9\%$$

The above are wideband fluctuations normalized with the local mean. These levels are not large compared to other wind-tunnels; see Figure 11, where the stream dynamic pressure q_∞ and tunnel-diameter Reynolds number $Re_{\infty D}$ are plotted. Equally important is the free-stream turbulence spectrum shown on Figure 12, whose great differences from Figure 9 confirm that the boundary-layer waves described herein are not obscured by the free-stream turbulence.

5. PHENOMENA IN THE TRANSITION ZONE

5.1 Variation of Mean Properties

Before tackling the observed laminar waves, we checked the cone boundary-layer to ensure that we had a well defined laminar flow before, and a well defined turbulent flow after the transition zone. Typical velocity profiles are shown on Figure 13. In the region where shadow-graphs show laminar flow, the profiles have the familiar linear (u/u_e vs. y/δ) profile, and they have the equally familiar $1/n$ (n large) exponential profile in the turbulent flow, where the shadowgraph shows turbulence. Similar confirmation exists from temperature, Mach number and other profiles (see Reference 2).

Closer spaced, albeit semi-qualitative, data clustered around the transition zone were reduced from Tape 65 and are shown on Figures 14, 15 and 16. Figure 14 shows hot-wire mean-voltage profiles (roughly proportional to ρu) at sequential stations through transition. By comparison with Figure 15, which displays similar data from quantitative measurements, it is clear that transition occurs by x = 39" (99 cm) from the cone tip. Similar data is shown for the local total flow temperature on Figure 16.

TABLE I

DEFINITIONS OF TRANSITION "BEGINNING" AND "END"
ADOPTED HEREIN

SENSOR or OBSERVED VARIABLE	"BEGINNING"	"END"
Wall temperature	Temperature first departs from a "constant" level	Temperature settles to "constant" level
Wall heat flux	Flux first departs from the "laminar" behavior	Flux settles to the dropping "turbulent" curve
Boundary layer thickness	Thickness stops growing as $(X/P_o)^{\frac{1}{2}}$	Thickness settles to a higher level
Spark shadowgraph	Random structure first observed	Structure is fully fine-grained
Laminar waves	First appearance of fluctuation peak in (hot-wire) spectrum	-
Hot-wire spectrum	Frequency peak of laminar waves first begins dispersing	Spectrum is completely random (no peaks)
T_o profile	Profile first departs from "laminar similarity"	Profile first collapses to "turbulent similarity"
ρu profile	As above	As above
Velocity profile	As above (first departure from near-linear profile)	As above (however, profile exponent is not 7 necessarily)

5

The conclusion from such displays (Figures 13-16) is that there are recognizable laminar and turbulent flows on either side of the transition zone.

5.2   The Mean (Average) Flow Phenomena in the Transition Zone

That the flow behaves normally in the transition zone is also evident from Figure 17. Here the flow to be considered in detail in this contract is examined from the viewpoint of surface temperature T_w and heat rate S_t as well as boundary-layer thickness growth δ, δ^* and θ.

Figure 17 (a) shows that the wall temperature remains very nearly constant then rises to a maximum and decays towards another constant level. The heat rate (Figure 17 (b)) displays the customary rise of the heat flux from the laminar to the turbulent values. The three types of boundary-layer thicknesses are shown on Figure 17 (c). The points should, for laminar flow, lie on curves of the type

$$\delta, \delta^*, \ \theta \sim x^{\frac{1}{2}}$$

which is shown true by the dashed lines. It is surprising that the data points do not depart from the laminar behavior until after $x = 39''$ (99 cm) from the cone tip.

Figure 18 is a summary of the boundary-layer transition beginning ("BEG.") and end ("END") as sensed by nine different methods involving six separate instruments - surface thermocouples, surface heat flux gages, shadowgraph, hot-wire anemometers, pitot tubes and total-temperature probes. The definition of "beginning" and "end" is clarified on Table I. The conclusions drawn from Figure 18 are: (1) laminar waves are the first to signal the transition process, far upstream from all other sensors, (2) probes immersed in the flow give a much shorter transition zone than surface thermal instruments, presumably because the vehicle material conductivity "spreads out" the transition zone, and (3) the boundary-layer thickness is the last to signal transition onset. The latter conclusion implies that once it appears, turbulence spreads towards the wall faster than towards the external flow.

5.3   The Fluctuating Flow in the Transition Zone

As seen from Figure 18 and Table I, the laminar waves appear considerable upstream of where transition is indicated by all other sensors. An overall view of the events preceding, including and following the laminar oscillations is given by Figure 19. Here we have plotted the spectra of the first power of the hot-wire signal (at the highest overheat used) extending to 320 KHz, for zero blowing and angle of attack ($\alpha = \lambda = 0$). At each x (or Re_x) position spectra were recorded at y intervals of 0.08 δ, starting at y = 0.12 δ, and set up in the Figure to give a three-dimensional view of intensity, frequency and distance from the wall. The spectrum nearest the wall (i.e., at y = 0.12 δ) lies on

6

the "far" side of each diagram, while the free stream appears nearest the reader. These are low-resolution spectra, each bordered on the left by a tall, broad "blip" marking zero frequency, and resting on a noise "baseline".

The "fundamental" oscillation first appears around $Re_x = 1.5 \times 10^6$ and is clearly and strongly formed by 2.6×10^6. A little later, at $Re_x \cdot 3.5 \times 10^6$ the second harmonic appears, and both peaks continue growing until about $Re_x = 4 \times 10^6$. At this point spectral dispersion begins, with a decrease of the oscillation intensity and the appearance of turbulence. The first harmonic is barely visible at $Re_x = 5.2 \times 10^6$, and finally the spectrum appears fully random at 5.5×10^6.

The quantitative surface heat rate and boundary-layer profile data taken simultaneously and discussed in the previous section, show that the surface heat flux first departs from its laminar level at $Re_x = 5.3 \times 10^6$ and attains a turbulent level at $Re_x = 7.2 \times 10^6$. Shadowgrams show transition as occurring roughly near $Re_x = 5.8 \times 10^6$. The velocity profile is still laminar-like at $Re_x = 4.84 \times 10^6$, but shows a 1/7 - law dependence at $Re_x = 6.5 \times 10^6$. The fluctuation intensities execute their spatial diffusion somewhere between these last two limits also.

There has been some question whether hypersonic transition is preceded by bursts, and a study was made of the instability waveform at $Re_x = 4.8 \times 10^6$, which is well after spectral dispersion begins and shortly before the surface heat rates first depart from the laminar value. It is quite clear that bursts exist superimposed on the periodic structure. Note that the latter is still visible as far away from the boundary-layer edge as $y = 1.84 \, \delta$. This is shown on Figure 20.

Figure 21 summarizes the growth of the oscillations and their dispersion by traversing the low resolution sensor at $y/\delta = 0.70$ in the region $2.3 \times 10^6 < Re_x < 6.5 \times 10^6$. In this rather condensed view the bursts are harder to distinguish from the noise, but the appearance and decay of the waves is clear. Note, too, that the "final" turbulence intensity is not perceptibly greater in amplitude than the periodic wave amplitude prevailing for some distance prior to transition. Modally-resolved high-resolution wideband fluctuation data as presented in References 2 and 3 confirm this phenomenon. For example, the wideband $T'/\overline{T}$ level at $y/\delta \simeq 0.7$ has already reached 0.25 as early as $Re_x = 3.2 \times 10^6$, which is about the maximum achieved later by $T'/\overline{T}$ through and after the transition zone. The detection of transition in the body of the boundary layer cannot be done precisely, therefore, without a full spatial, modal and Fourier resolution of the hot-wire signal.

5.4 The Amplification Rates of Laminar Oscillations

The school of thought built around stability theory likens the laminar boundary layer to an "amplifier" receiving as "input" small disturbances

from upstream (e.g. stream turbulence, wakes of roughness elements, etc.) and producing as "output" large oscillations which break up into turbulence. Transition can be delayed or hastened depending on the magnitude and spectrum of the input and the "gain" of the amplifier. If the gain is known, then transition can be predicted from the flow disturbance inputs given for specific flight applications or wind tunnel experiments. According to classic stability theory and its extension by L. Mack to the present case (Reference 4), the gain is so selective that along a given boundary layer streamline some fluid fluctuations amplify while some others damp.

Recent results on this contract are shown on Figures 22 through 25, as obtained from the Tape No. 65 playback. Coordinates have been made non-dimensional for direct comparison with the Mack theory and the Kendall experiments. Thus in Figure 22 we show the amplification rate

$$- \alpha_i = \frac{1}{2A} \frac{dA}{dR}$$

as a function of streamwise distance along the body or its equivalent

$$R = \sqrt{Re_x} \sim \sqrt{x}$$

where Re_x is the Reynolds number based on the unit Reynolds number R_e' at the boundary layer edge (in this case $Re' = 65,400$ cm^{-1}) and the distance x from the sharp cone tip. The quantity A is the spectral density (e.g. volts/Hz) of the sensor output for a given frequency f; the latter is also made non-dimensional using the constants Re', as above, and the edge velocity u_e (=1,136 m/sec):

$$F = \frac{2\pi f}{u_e Re'}$$

Figure 22 thus says, for example, that a disturbance of frequency f = 100 KHz (F = 0.845 x 10^{-4}) amplifies (positive - α_i) in the region upstream of x = 73 cm (or R=2190) from the cone tip, and damps (negative - α_i) in the region downstream of the same x.

An "amplification" spectrum is plotted from these data on Figure 23 which is very similar to that obtained by Kendall (compare Figure 23 with Figure 12 of Reference 5). As on Figure 22, these data are for a hot-wire traversed at $y = 0.8\delta$ (chosen because the signals are strong there) in the following ranges:

x = 19" to 39" (48 to 100 cm) which means R from
1776 to 2545

f = 20 to 260 KHz which means F from 0.169 x 10^{-4}
to 2.197 x 10^{-4}

8

Figure 23 shows that at all positions R on the cone the low and high frequencies amplify, with damping at the intermediate frequencies.

These data have been recast into the familiar "stability diagram" of Figure 24. The diagram delineates regions of amplification and damping in the F-R plane, separated by neutral boundaries, and also shows the lines of maximum amplification. The data of Kendall (edge Mach No. M_e = 7.7, wall temperature T_w = 0.6 T_o) are compared with ours, (M_e = 7, T_w = 0.75 T_o) since the conditions in the two tests are nearly identical. The agreement is very good, the only discrepancy being in the upper neutral branch. What this picture shows is largely an amplification region with a narrow "corridor" of damping extending roughly from F = 2 x 10^{-4}, R = 1400 to F = 0.8 x 10^{-4}, R = 2400. The neutral boundaries then separate two amplification regions of a shape reminiscent of those observed on flat plates at lower Mach numbers (see, for example, Figure 16.8 of Reference 9. According to these early results, a line of "maximum" amplification should lie close to the upper neutral boundary of the amplification region as seen on Figure 24. This lower amplification region is associated with the optically detected waves and the largest peak in the hot-wire spectra (see Figures 5 and 7). The upper region, lying above the upper neutral boundary on Figure 24, is connected with the "second harmonic" seen in the spectra. It is speculated that if more data are available to fill the lower R region, and especially the higher F regions of Figure 24 (say F > 2 x 10^{-4}) more stability regions will be found. In fact, a hint of a third neutral boundary is shown on the upper right hand side of the data on Figure 24. Finally, a puzzling feature of Figure 24 is the existence of two lines of maximum amplification at the bottom of the Figure; as will be seen below, it is suspected that the lowest maximum amplification line shown is due to inclined first-mode waves. Another is that even the lowest frequencies amplify in the range 1800 < R < 2400.

The black cross on Figure 24 marks the frequency of maximum amplification for second-mode waves from the theory of L. Mack (Reference 4). For perfect agreement, the cross should lie on the dashed line immediately above it. This comparison with stability theory is better shown on Figure 25, which re-draws an isolated case from Figure 23. The agreement with Mack's theory is good, both as regards the location of the most amplified frequency and as regards the magnitude of the amplification.

6 DISCUSSION

The surprise initially created by the clarity and ease of detection of the instabilities at these hypersonic conditions stems from the difficulties met in earlier experiments done at supersonic speeds (References 6,7). In this earlier case the theory predicts lower amplifications for the second mode and a higher susceptibility of interaction with and masking by wind-tunnel stream turbulence, e.g., sound radiation. Also, at $1 < M_e < 5$ the density gradients in the layer are correspondingly lower, while velocity oscillations u' there give density fluctuations ρ' which are relatively low:

$$\rho' \sim (\gamma - 1) M^2 u'$$

At hypersonic speeds, say $5 < M_e < 10$, the theory predicts higher amplifications and weaker coupling between instabilities and extraneous noise from the wind-tunnel flow. Furthermore, the higher M creates large density gradients across the layer and larger density fluctuations for a given velocity fluctuation within it. The point made here is that at hypersonic speeds the instability events observed are both more pertinent to transition and clearly easier to measure. This regime is, of course, also the one of current interest in flight applications.

There is also much interest in relating the surface flux phenomena to the actual transitional phenomena in the flow. La Graff has found that the maximum in the gross (raw) wideband signal of the hot-wire as the latter is traversed along the layer (presumably at constant y/δ) coincides with the point of "beginning" transition as sensed by surface heat flux sensors (Reference 8). The present findings are somewhat different: the only important coincidence found here is the disappearance of the first harmonic peak (i.e., total Fourier dispersion or "randomization") with the "beginning" transition as sensed with the surface heat flux. And, if one concentrates exclusively at the physical (e.g. $y/\delta \sim 0.70$) and Fourier (e.g., $f \sim 2\, u_e/\delta$) space region where the "action occurs", then one sees little of any maximum in the fluctuation intensity as the sensor is swept through the transition zone.

7. CONCLUSIONS

The following can be concluded from this experimental work:

1. There exists an intense, omnipresent wave structure through the laminar and transitional boundary layer on the cone model, which is apparently two-dimensional in character. The waves are concentrated near the layer edge and are moving relative to the surface, with a wavelength of slightly in excess of $2\,\delta$.

2. The waves are not grossly affected by moderate angle of attack, surface mass injection rates or wind-tunnel turbulence. In a physical sense the waves are made up of density crests and valleys as opposed to velocity fluctuations; as many as three harmonics, including the fundamental, have been observed.

3. The waves have been found to cause transition to turbulence by temporal, spatial and Fourier dispersion, in the form of bursts, diffusion toward the surface, and spectral dilution toward a random structure.

4. Other sensors employed place the transition onset considerably downstream from where the laminar waves were first seen. Surface sensors yield a much wider transition zone than sensors held in the boundary layer away from the wall.

10

8. RECOMMENDATIONS ON CONTINUED WORK

Although the processing of the present AEDC tapes is by no means complete, areas have been identified where further experimentation is necessary, especially to obtain data not presently on hand.

a) The height of the peaks shown on Figure 19 are plotted vs. distance from the cone tip on Figure 26. Note the increase and subsequent decay of the fluctuations, and also that the two curves (at P_O = 150 and 350 psia) do not seem to coincide. Therefore, data should be obtained at M_∞ = 8, P_O = 250 psia (Re_∞' = 37,000 per cm). These will enable us to bridge the gap shown on Figure 22 between the 150 psia and 350 psia data. It is important that, in addition to the data on hand, we have information at constant unit Reynolds number spanning completely the region from zero laminar waves to the fully turbulent case.

b) The effect of wall temperature on the stability should be examined. Lately, claims have been made about repeated stabilization and destabilization of the boundary layer as the surface temperature continues dropping. This is an important effect claiming a role in the so-called "transition reversal" phenomenon. We have a suitable model (4° half-angle cone) which can be internally cooled and can be used to study the instabilities with the cooled-wall condition.

11

REFERENCES

1. Martellucci, A. and Laganelli, A., "Hypersonic Viscous Flow over a Slender Cone, Part I: Effect of Reynolds Number, Blowing and Angle of Attack on Viscous Layer Properties", AIAA 7th Fluid and Plasma Dynamics Conference, Palo Alto, California, June 17-19, 1974.

2. Laderman, A.J., "Hypersonic Viscous Flow over a Slender Cone, Part II: Turbulence Structure of the Boundary Layer", AIAA 7th Fluid and Plasma Dynamics Conference, Palo Alto, California, June 17-19, 1974.

3. Laderman, A.J., "Effect of Mass Addition and Angle of Attack on the Hypersonic Boundary Layer Turbulence over a Slender Cone", SAMSO TR 73-397, Los Angeles, California, September 1973.

4. Mack, L.M., "Boundary Layer Stability Theory", Document 900-277, Rev. A, Jet Propulsion Laboratory, California Institute of Technology, Pasadena, California, 1969.

5. Kendall, J.M., "Wind-Tunnel Experiments Relating to Supersonic and Hypersonic Boundary Layer Transition", AIAA Paper No. 74-133, AIAA 12th Aerospace Sciences Meeting, Washington, D.C., January 30, 1974

6. Laufer, J. and Vrebalovich, T., "Stability and Transition of a Supersonic Laminar Boundary Layer on an Insulated Flat Plate", Journal of Fluid Mechanics, Vol. 9, Part 2, 1960, p. 257.

7. Demetriades, A., "An Experiment on the Stability of Hypersonic Laminar Boundary Layers", Journal of Fluid Mechanics, Vol. 7, Part 3, March 1960, p. 385.

8. La Graff, John E., "Observations of Hypersonic Boundary-Layer Transition Using Hot-Wire Anemometry", AIAA Journal, Vol. 10, No. 6, June 1972, p. 762.

9. Schlichting, H., "Boundary-Layer Theory", McGraw-Hill Book Co., Inc. New York 1955.
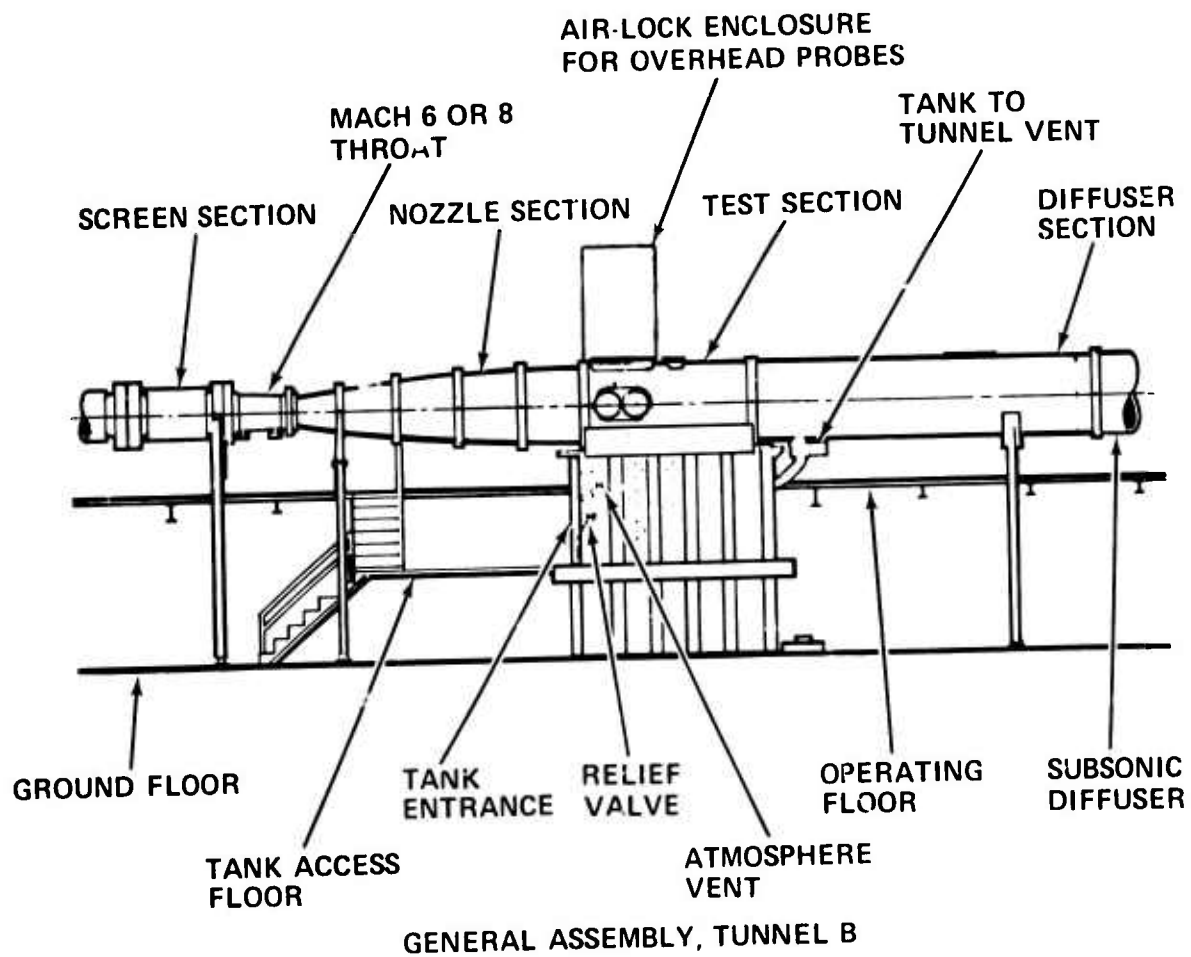
FIGURE 1

WIND-TUNNEL AT AEDC

13
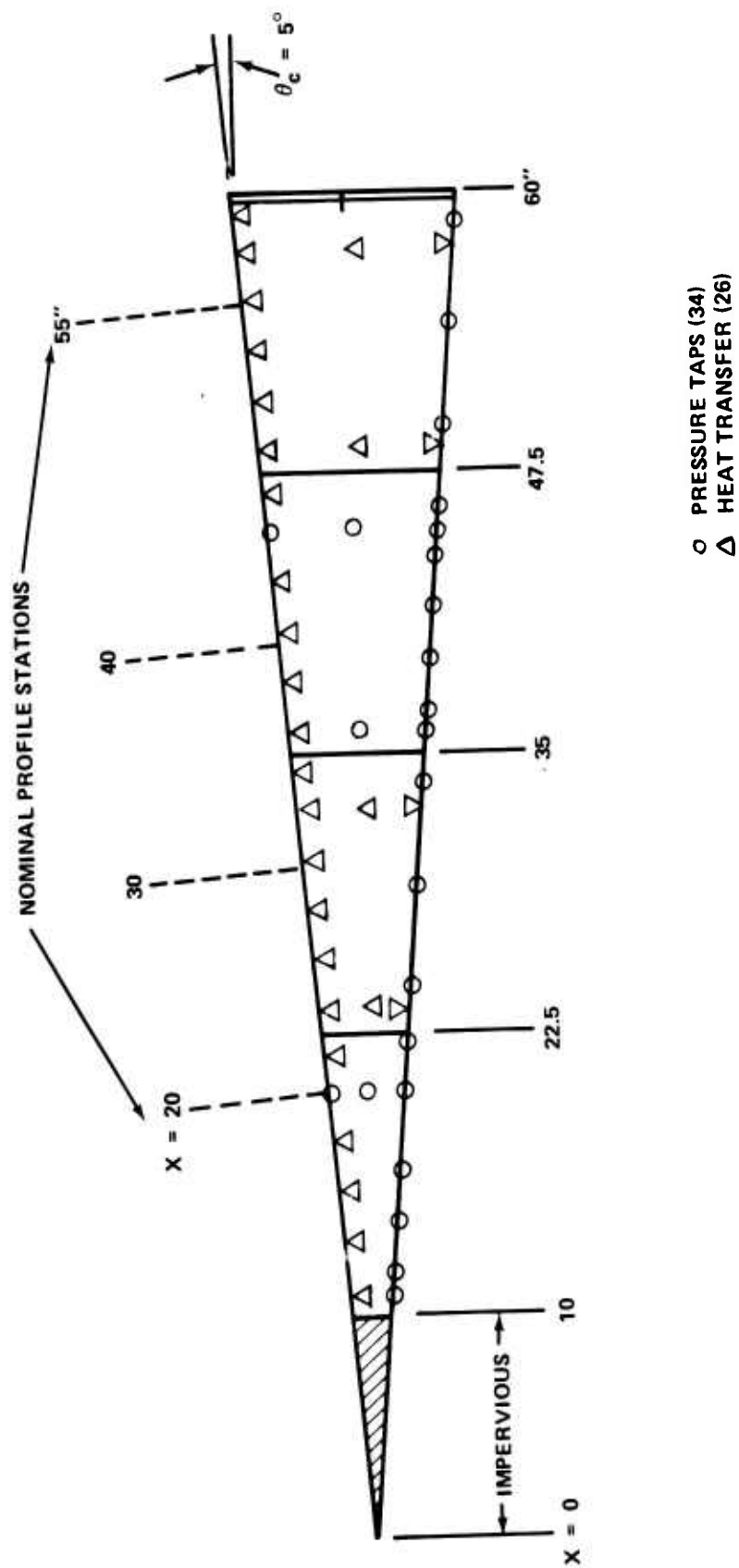
FIGURE 2

CONE-MODEL USED IN THIS EXPERIMENT

○ PRESSURE TAPS (34)
△ HEAT TRANSFER (26)

14

FIGURE 3
VIEW OF MODEL AND RAKE DURING TUNNEL RUN

15

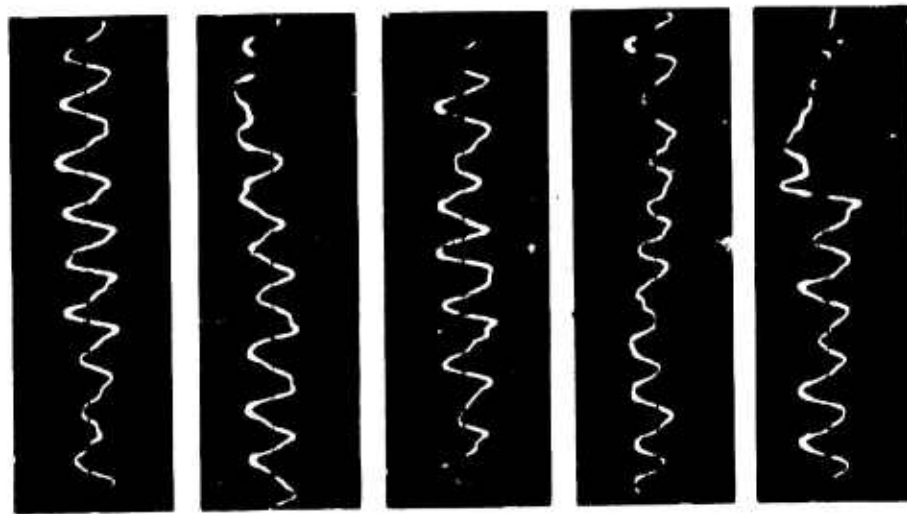FIGURE 4
ANALOG DATA ACQUISITION AND RECORDING CIRCUIT
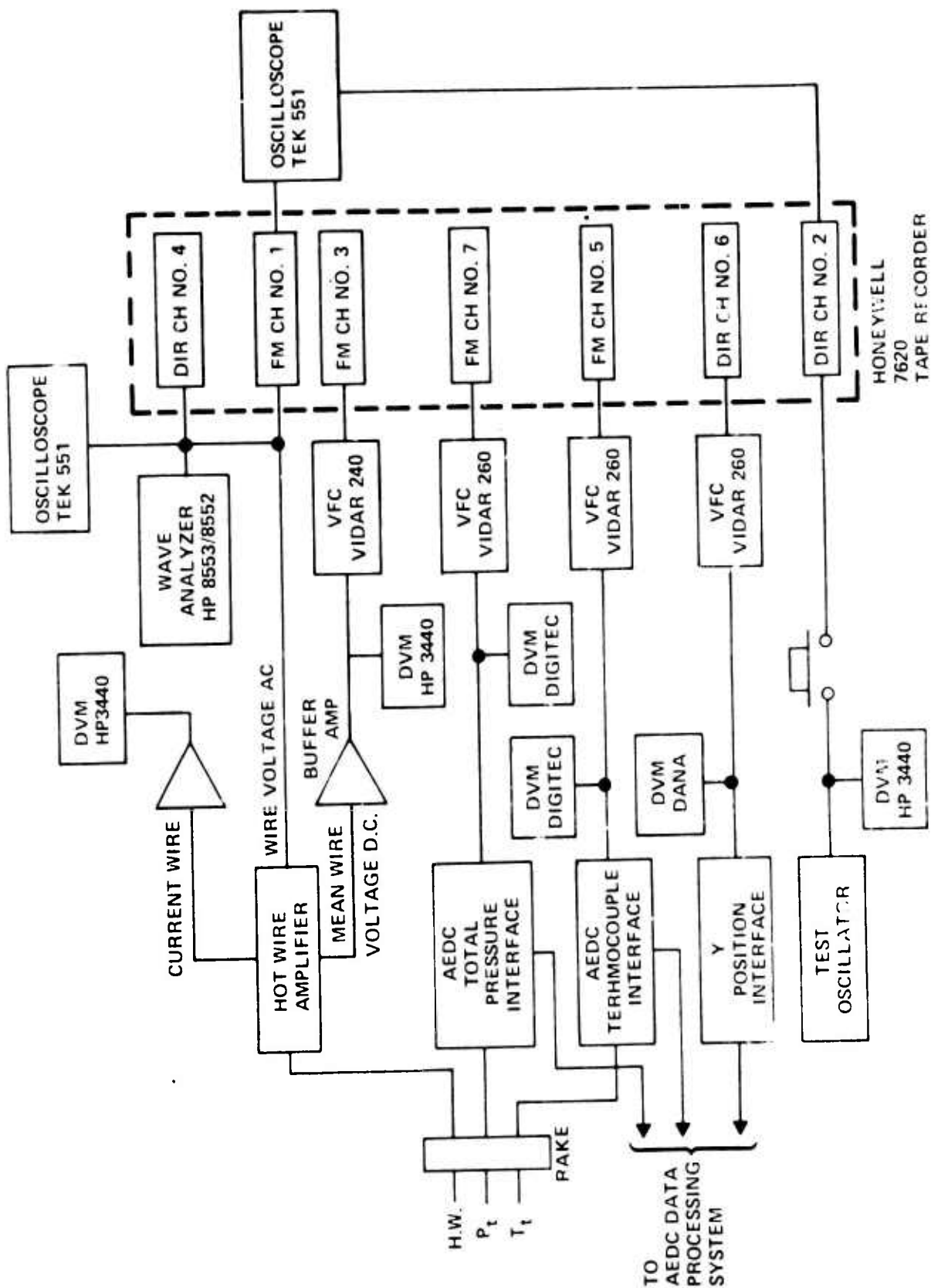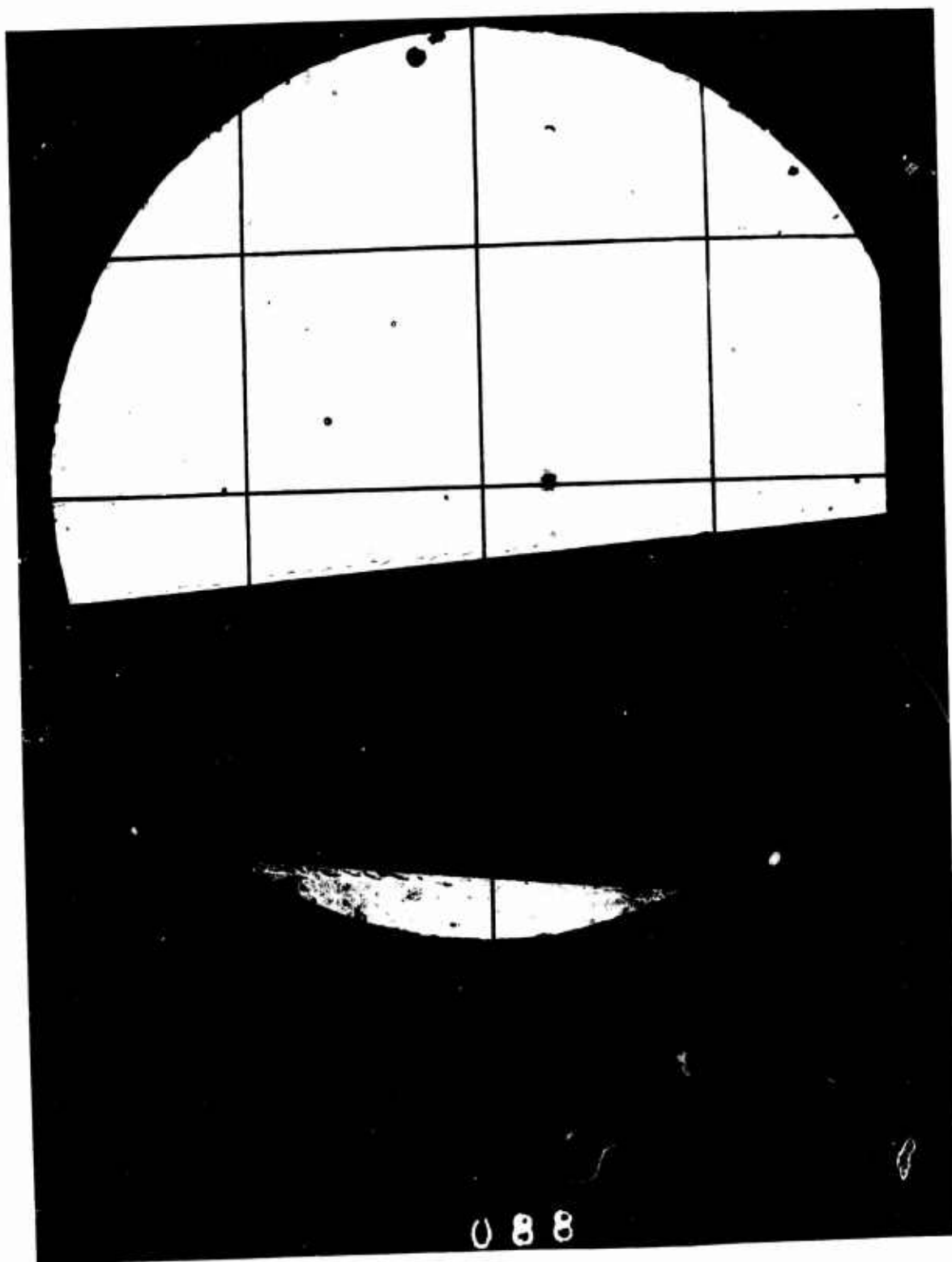
FIGURE 5
SHADOWGRAM OF THE LAMINAR WAVES

17

TEST: TBL-C
MODEL: 5-DEG. POROUS CONE (GE)
ORGANIZATION: PHILCO-FORD
FACILITY: AEDC/B
DATE: OCTOBER 1972
$M_\infty = 8.0$
$M_e = 7.0$
$P_o = 350$ PSIA
$T_o = 850\ ^\circ F$
$\alpha = 0^\circ$
$\lambda = 0$
$x = 19$ INCHES
$y \doteq \delta/2$
HOT-WIRE NO.: 56A   (0.00005 IN.)
Re/IN. = 141,000
$\delta = 0.29$ IN.
$\delta^* = 0.09$ IN.
$\theta = 0.0037$ IN.
$Re_\theta = 617$

|← 6.2 μSEC

FIGURE 6

TYPICAL OSCILLOGRAMS OF THE HOT-WIRE OUTPUT

18

$\longrightarrow$|12.5 μSEC|

$\frac{y}{\delta}$ = 0.44

$\frac{y}{\delta}$ = 0.75

$\frac{y}{\delta}$ = 0.97

NOISE

$\frac{y}{\delta}$ = 1.18

$\frac{y}{\delta}$ = 1.41

$\frac{y}{\delta}$ = 1.85

LAMINAR INSTABILITY WAVES

X = 19.1 IN., M_e = 6.945, Re'_∞ = 55,000 CM^{-1}

Re_x = 3.2 X 10^6, Re'_e = 65,700 CM^{-1}, R_θ = 618

u_e = 1138 m/SEC (UNFILTERED SIGNALS)
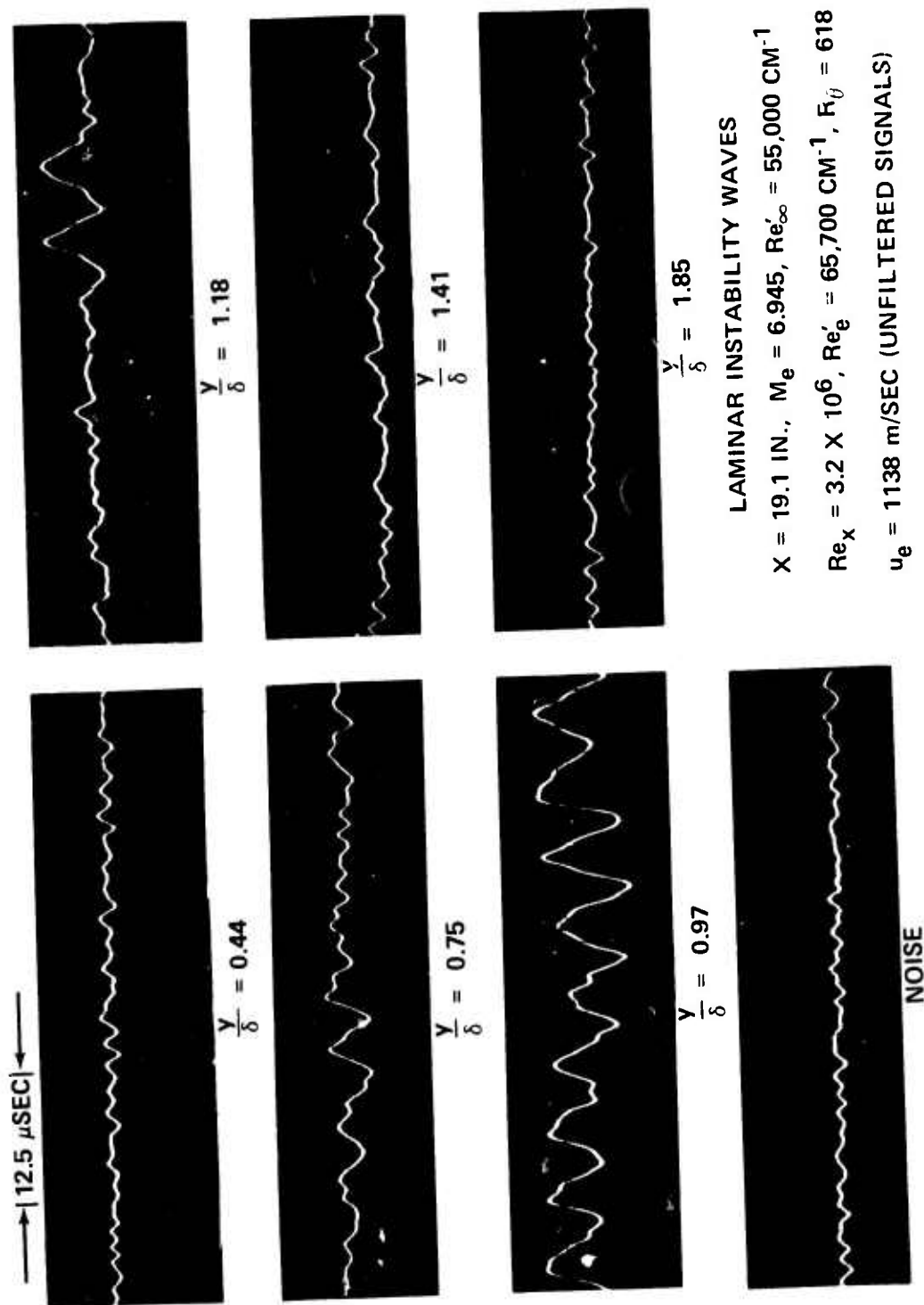
OSCILLOSCOPIC STUDY OF CHANGES IN THE WAVE CHARACTER ACROSS THE BOUNDARY LAYER

19
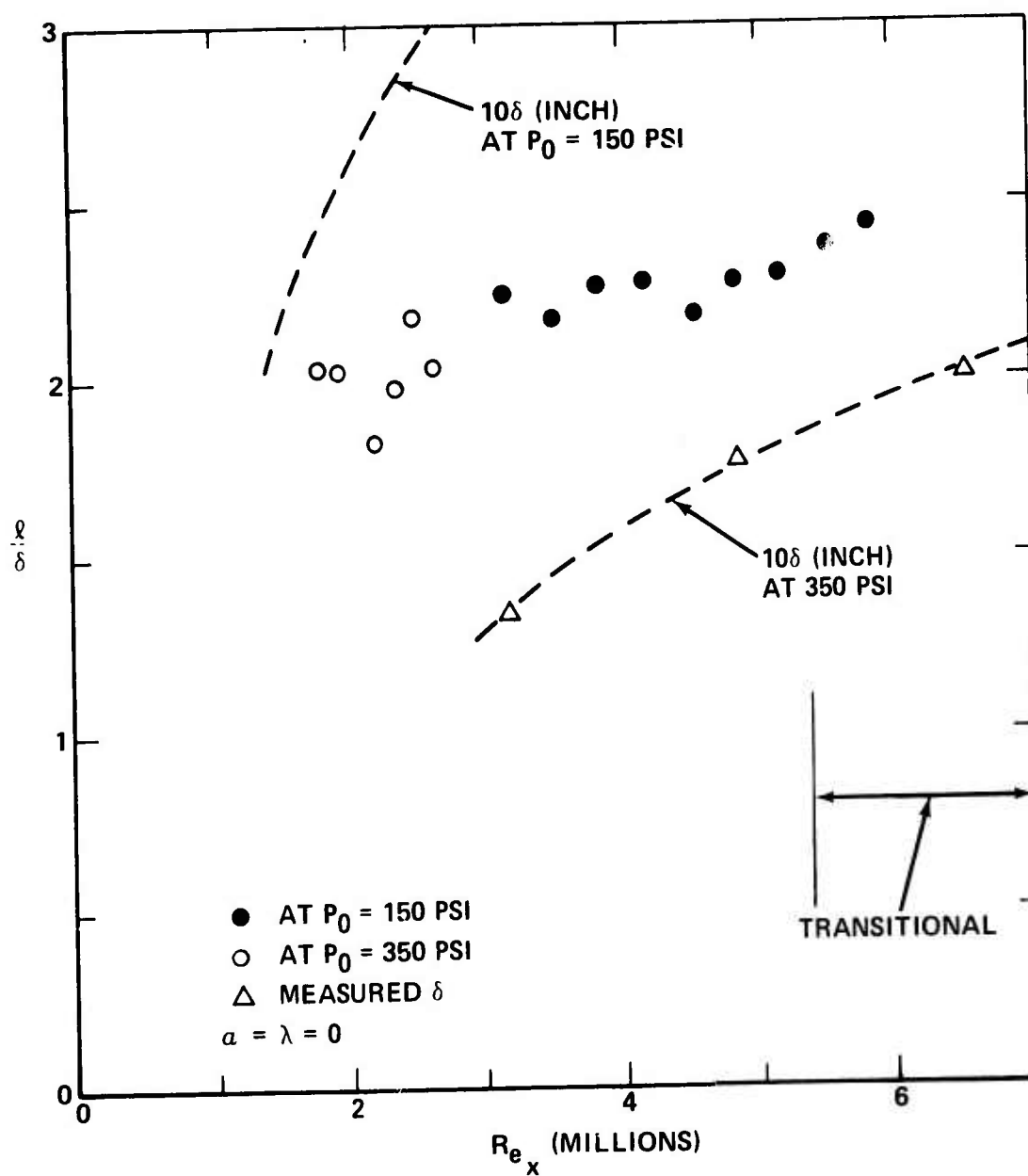
FIGURE 8

VARIATION OF NON-DIMENSIONAL WAVELENGTH
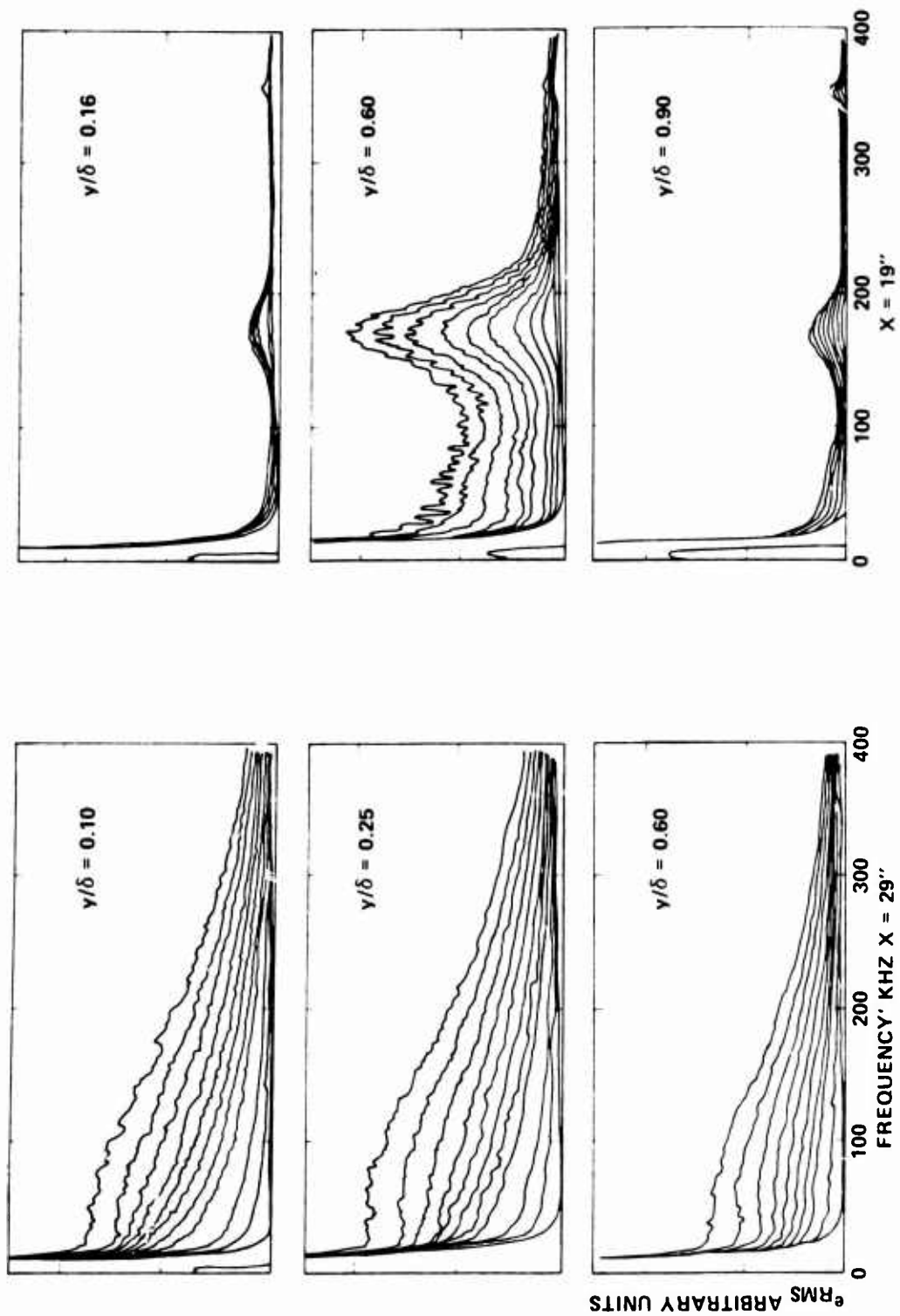
HIGH-RESOLUTION ENERGY SPECTRA OF THE HOT-WIRE OUTPUT IN A TYPICAL CASE

21
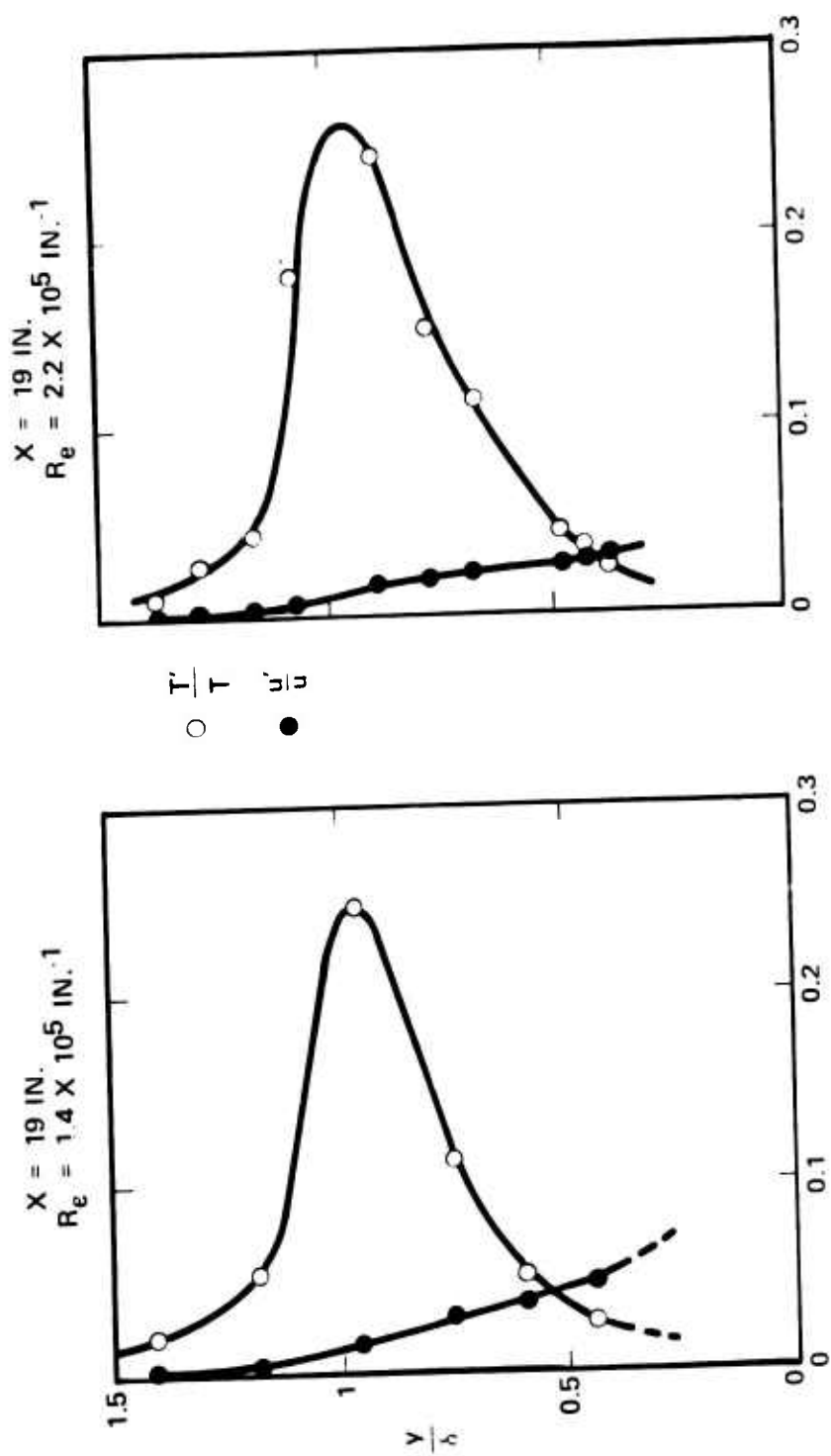
FIGURE 10

TYPICAL VARIATION WITH y/δ of the WIDEBAND VELOCITY AND TEMPERATURE FLUCTUATIONS

22
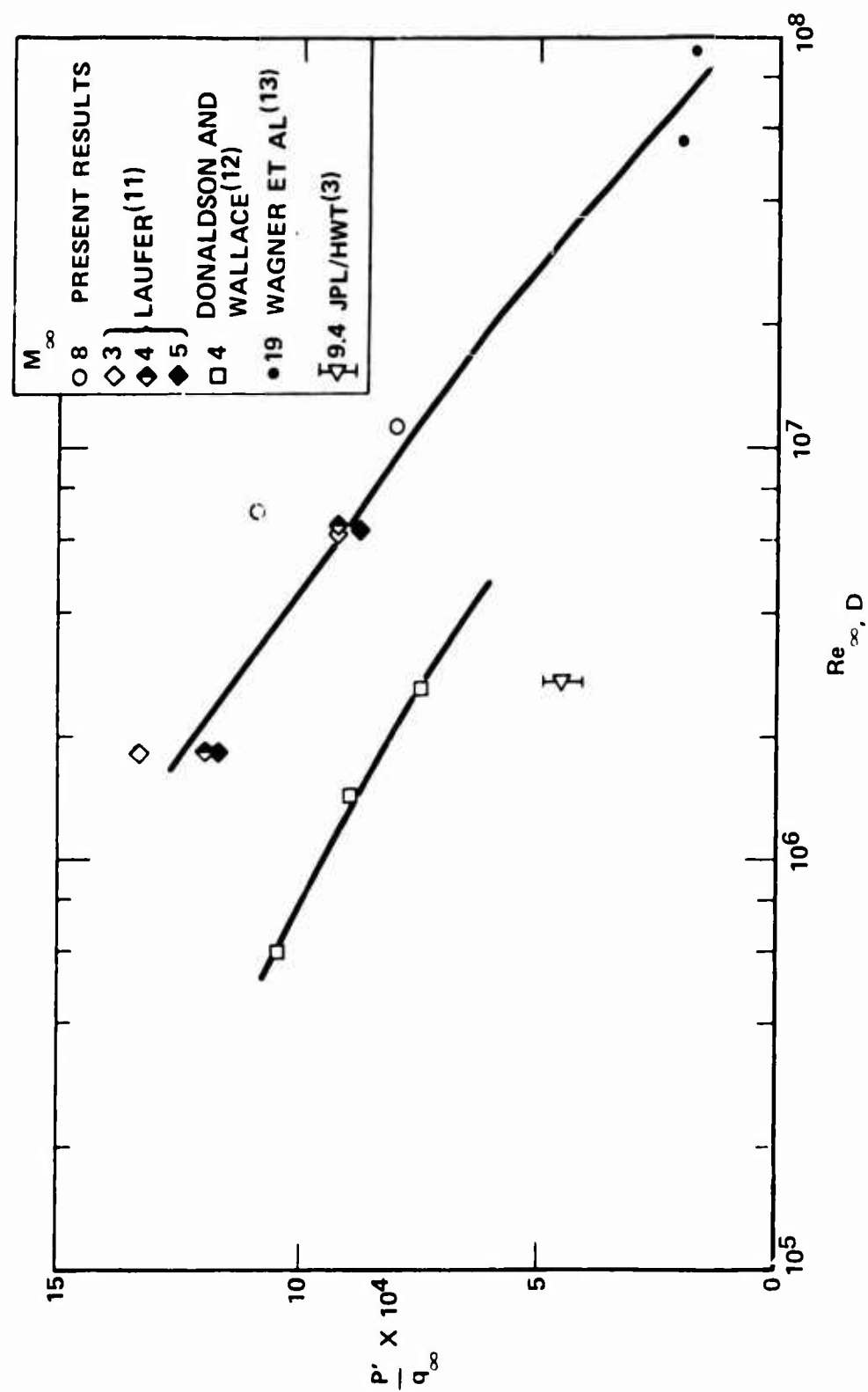
FIGURE 11

VARIATION OF TOTAL RMS PRESSURE FLUCTUATIONS WITH REYNOLDS NUMBER BASED ON
FREE-STREAM CONDITIONS AND TEST SECTION SIZE
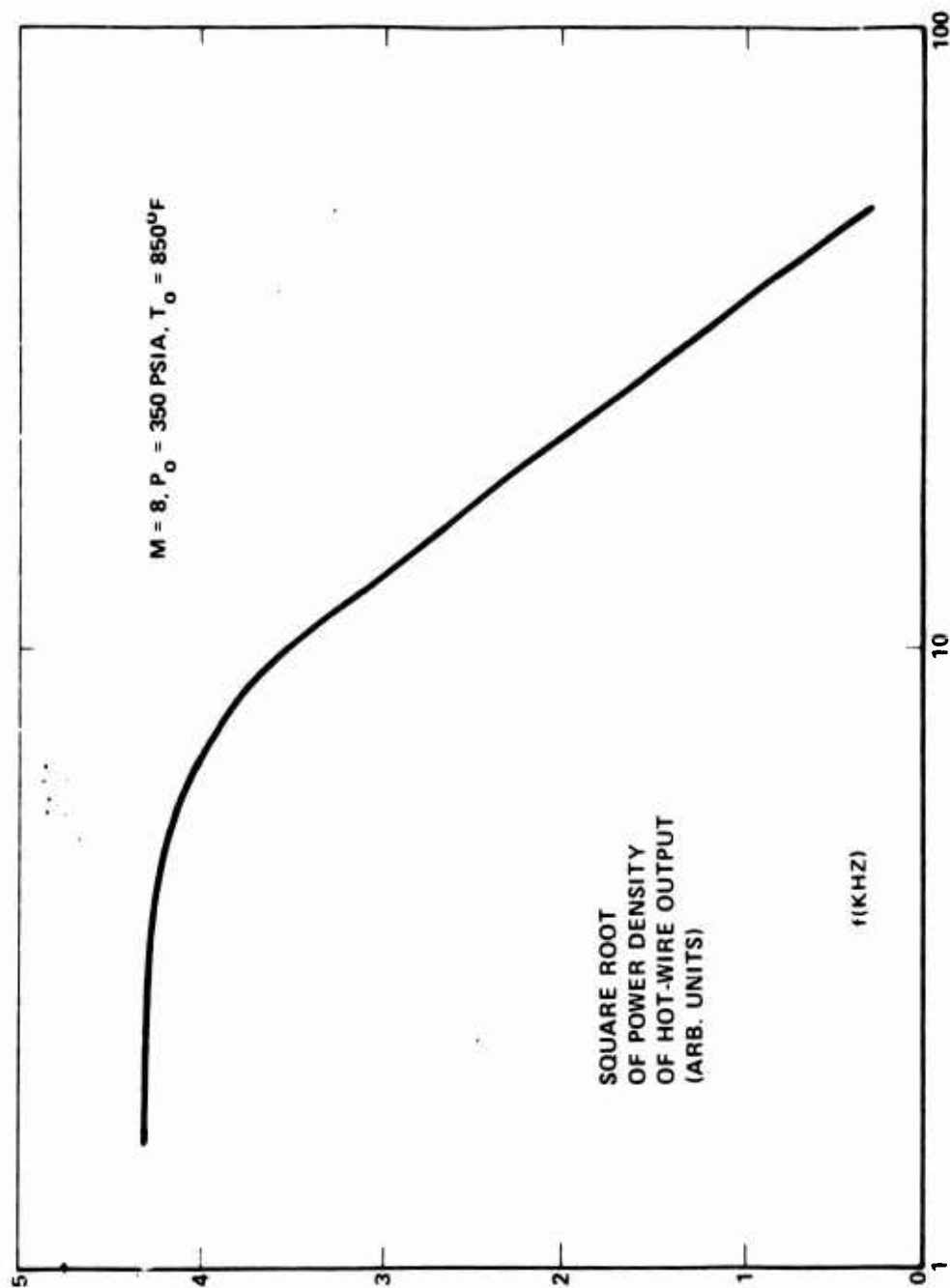
FIGURE 12

SPECTRUM OF FREE-STREAM TURBULENCE IN THE AEDC/B WIND-TUNNEL
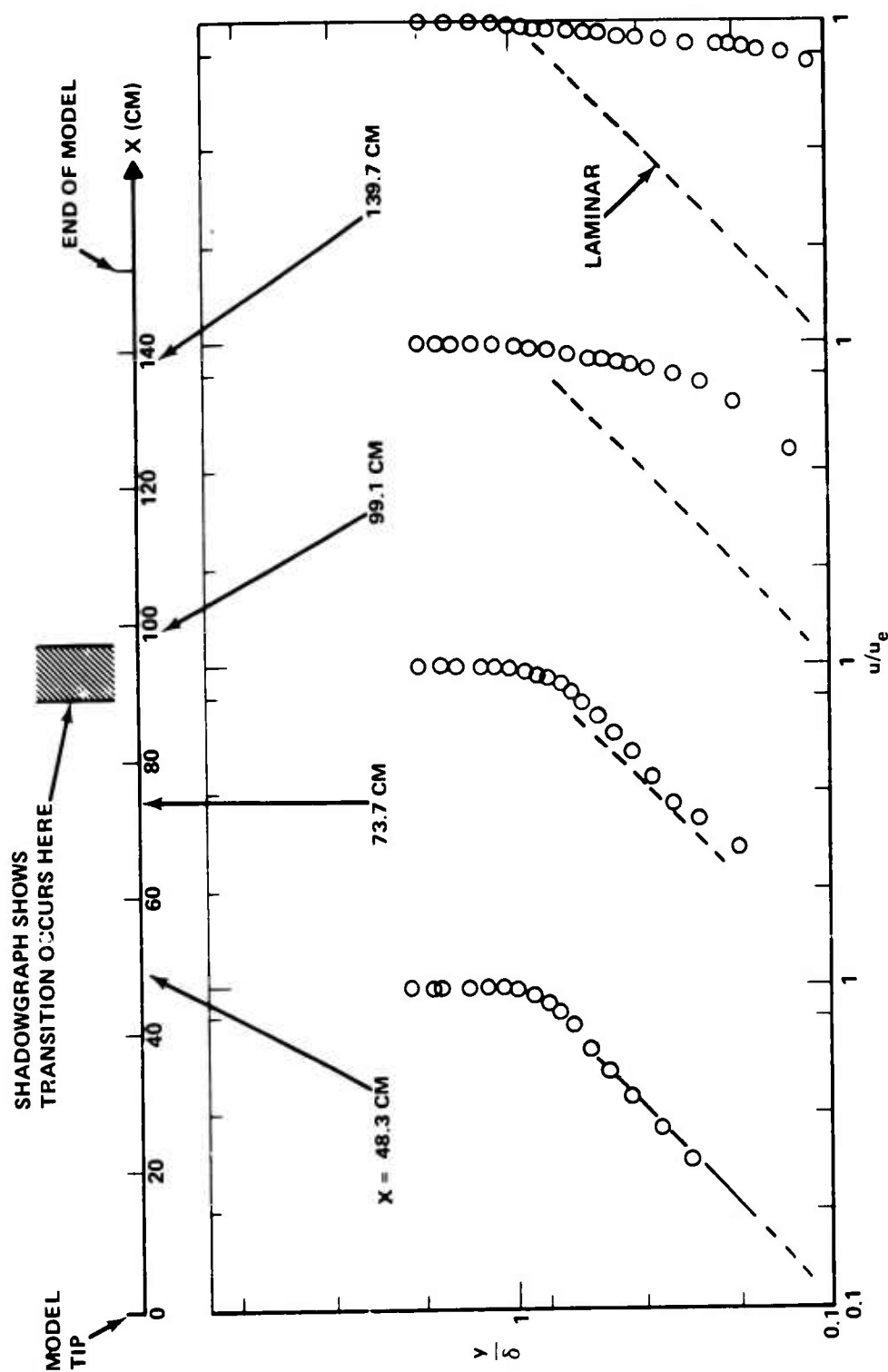
FIGURE 13

COMPARISON OF TRANSITION LOCATION DETECTED BY
SHADOWGRAPH AND VELOCITY PROFILE METHODS
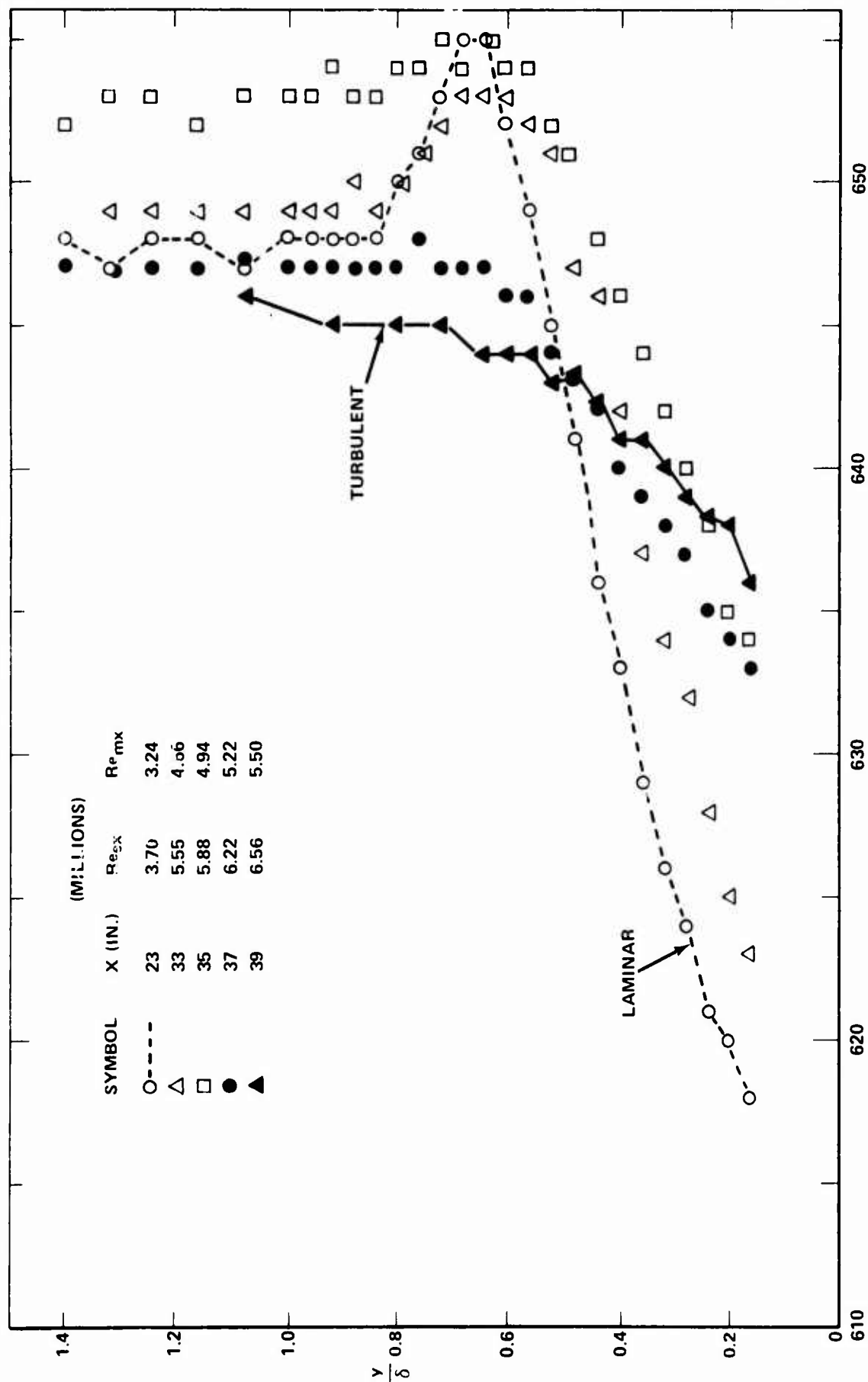
FIGURE 14

MEAN OF WIRE VOLTAGE VS. X, PROPORTIONED TO ~ u

26
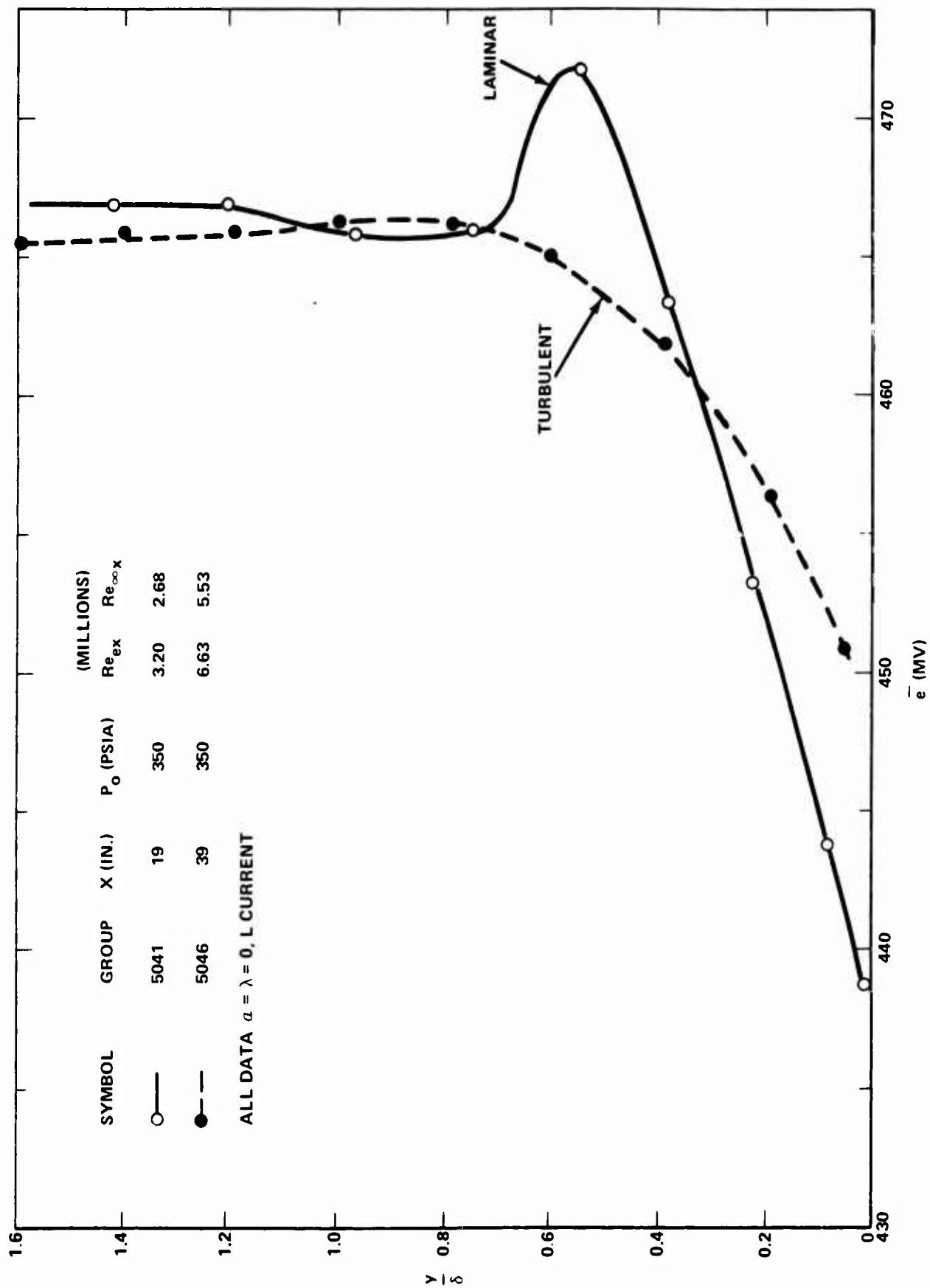
FIGURE 15

WIRE VOLTAGE PROFILES, LAMINAR VS. TURBULENT, QUANTITATIVE
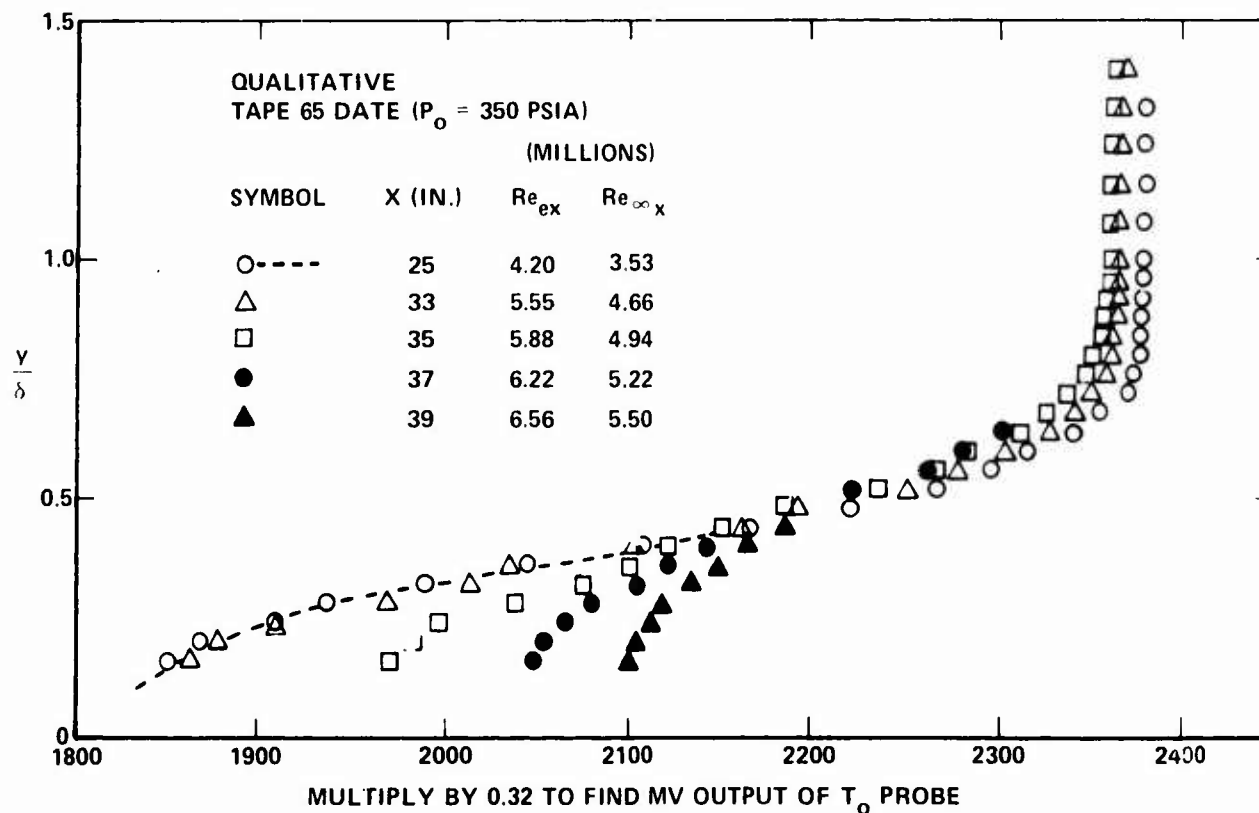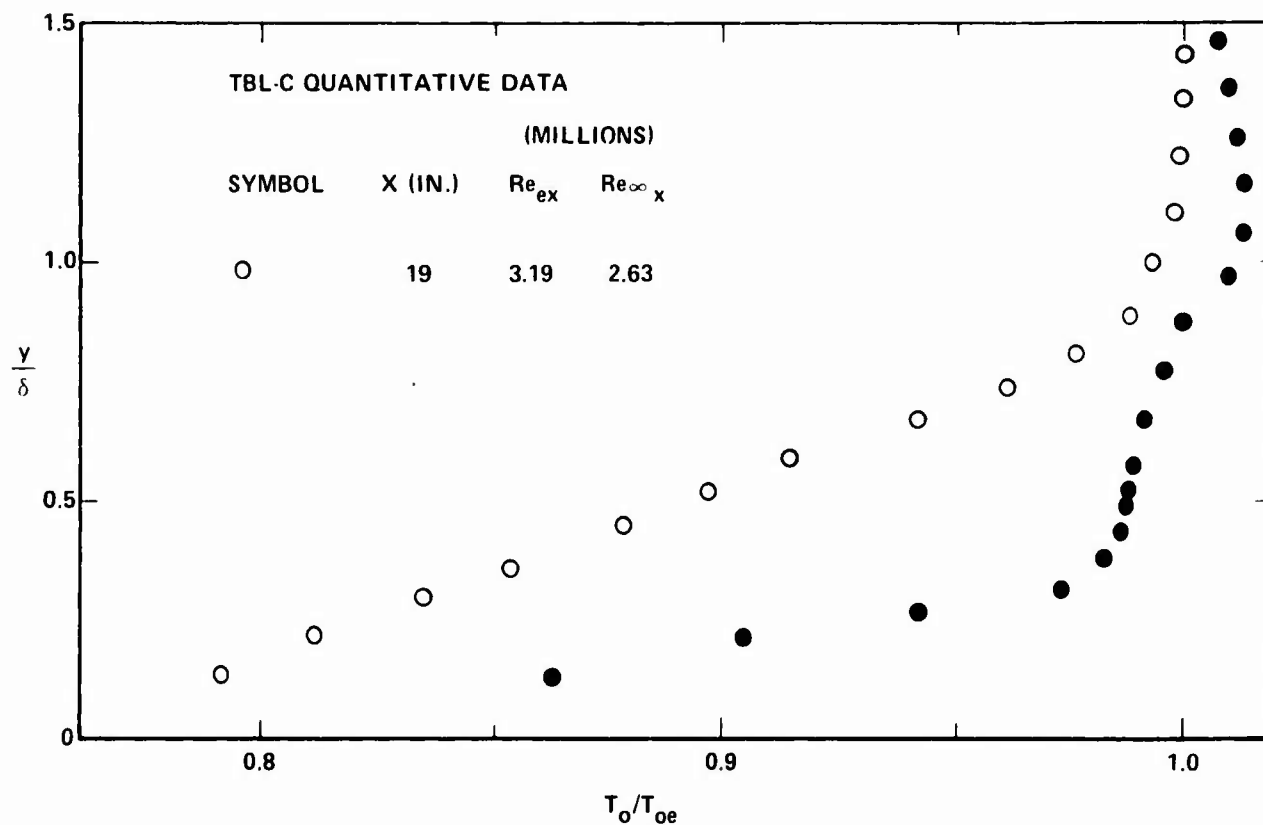
FIGURE 16
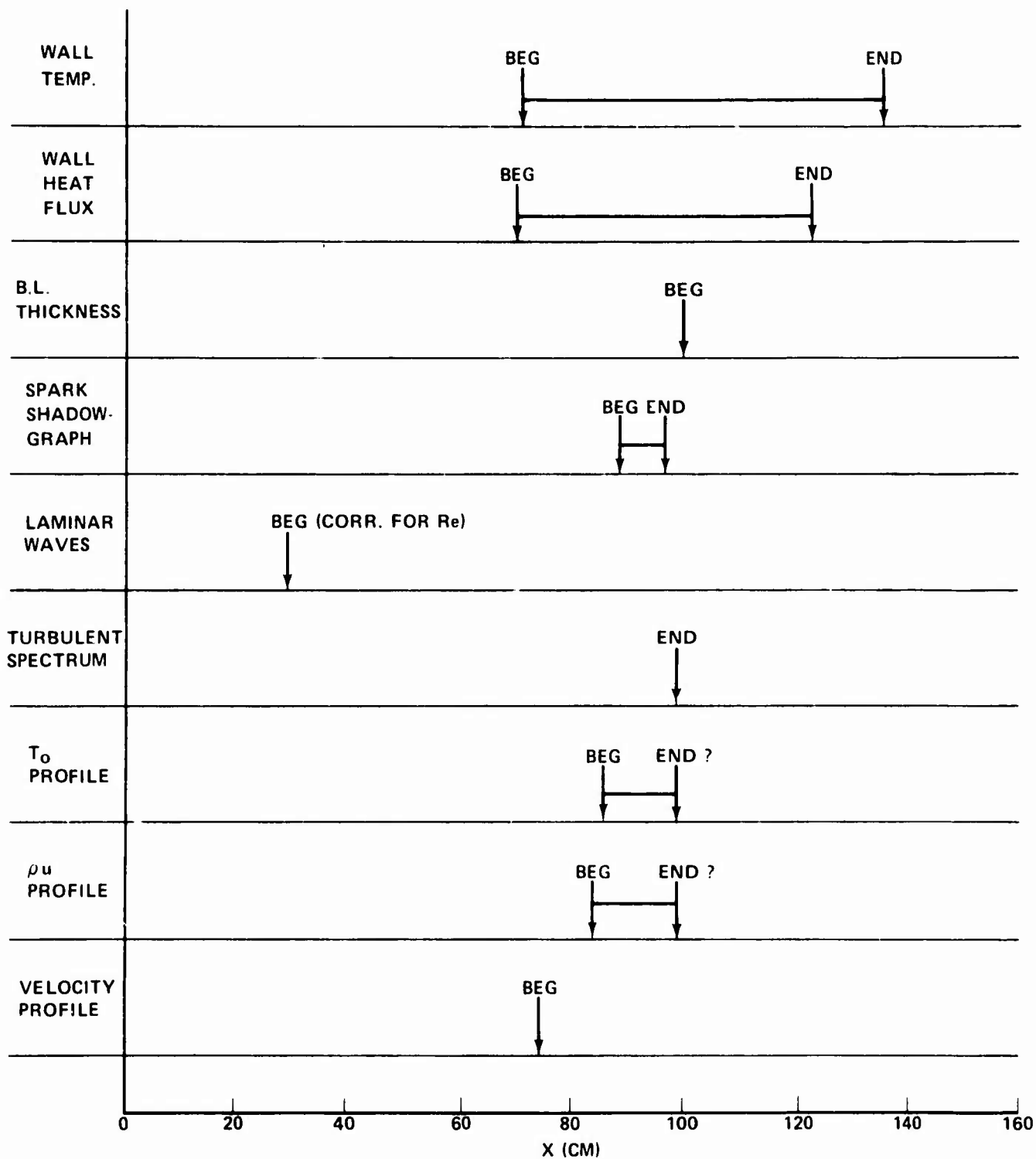
T_O - PROBE OUTPUTS IN TRANSITIONAL REGIME

28
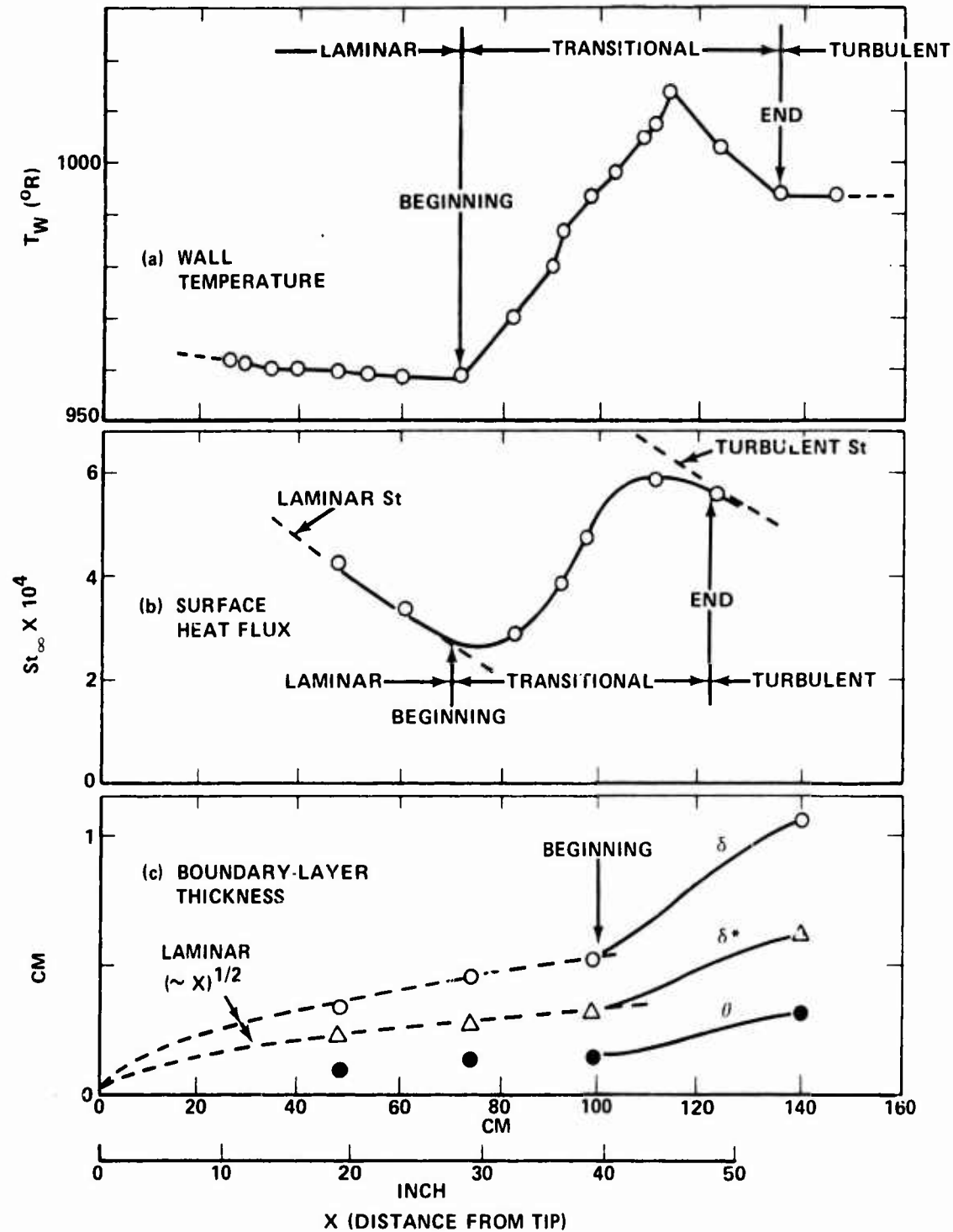
FIGURE 17

SURFACE TEMPERATURE AND HEAT FLUX, AND BOUNDARY-LAYER
THICKNESS

FIGURE 18

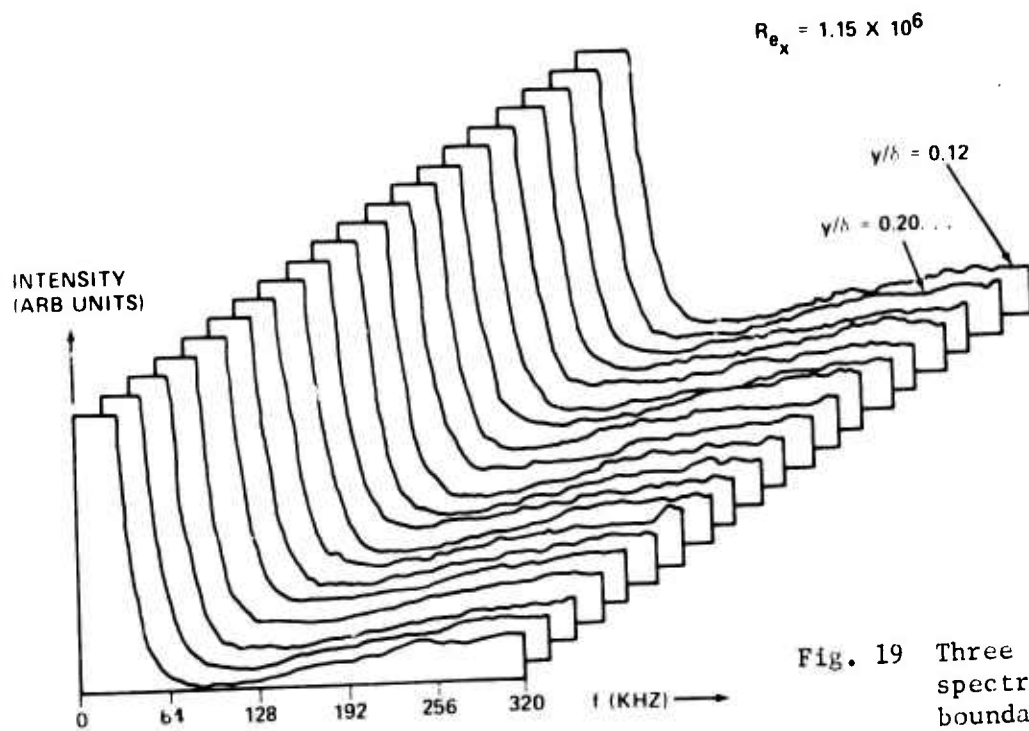TRANSITION INDICATIONS FOR VARIOUS SENSING METHODS (P_0 = 350psia)

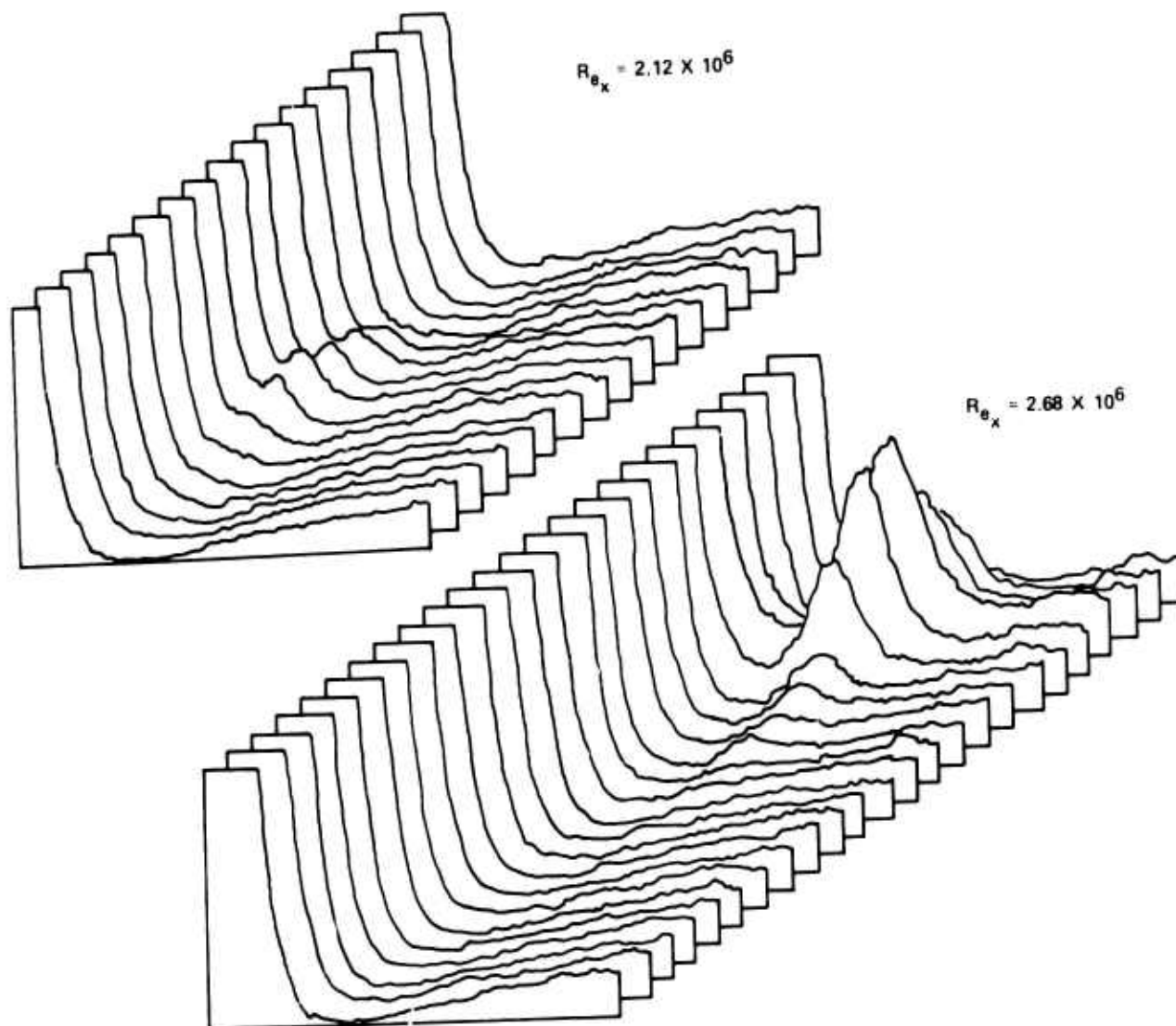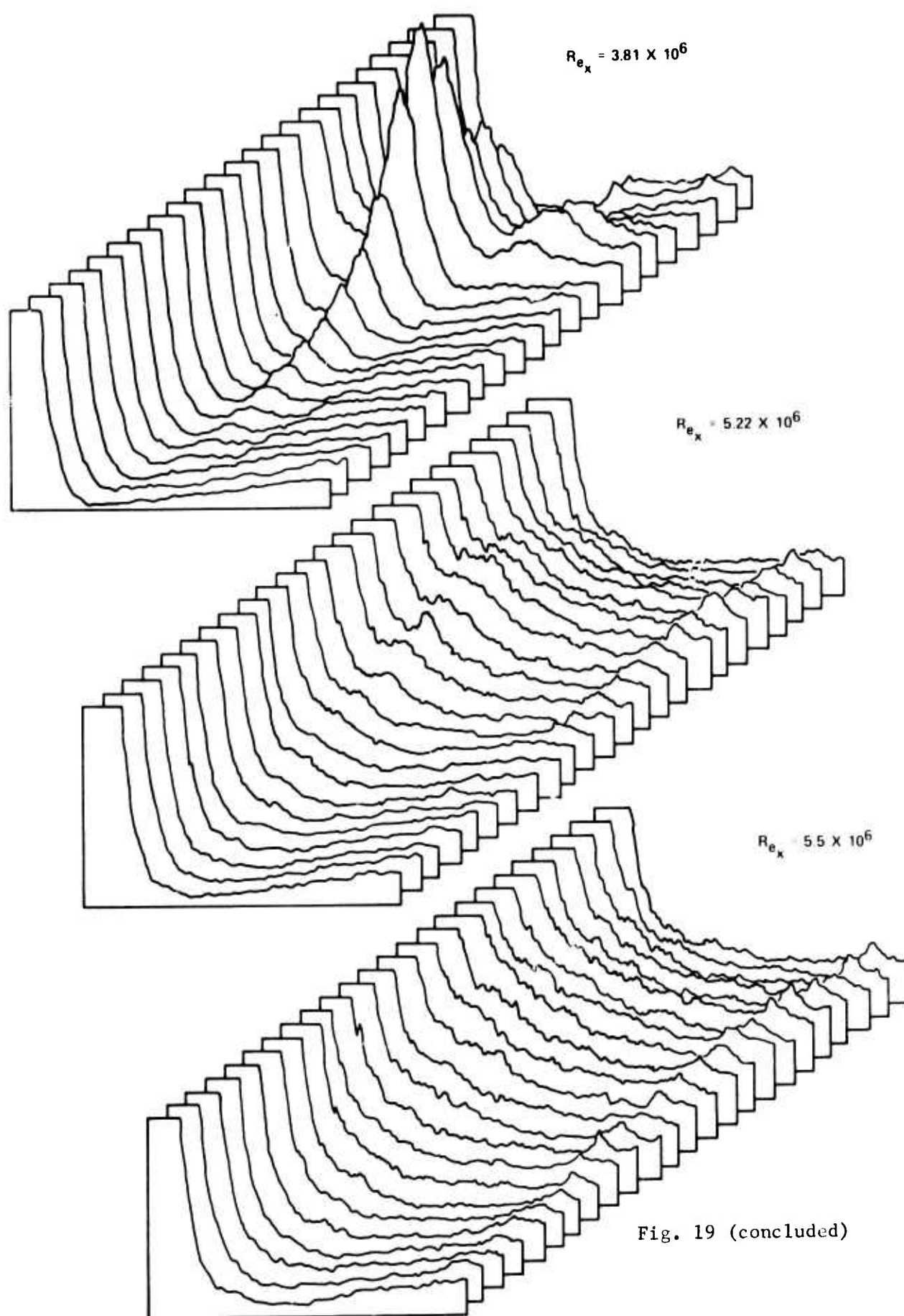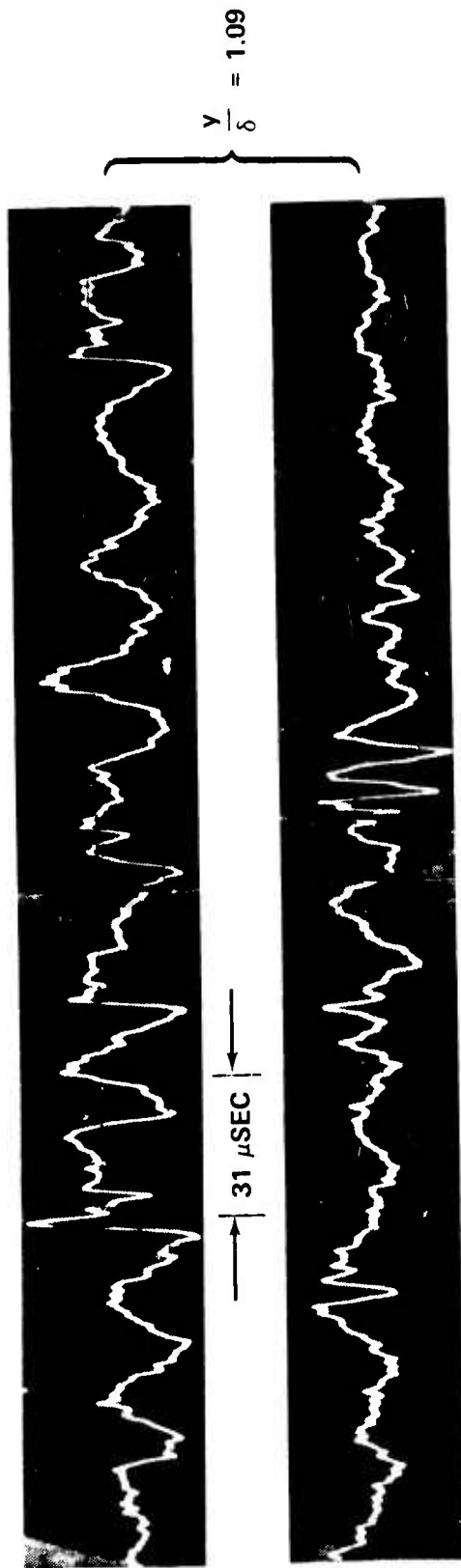Fig. 19   Three dimensional view of spectrum evolution in the boundary layer

$R_{e_x} = 3.81 \times 10^6$

$R_{e_x} = 5.22 \times 10^6$

$R_{e_x} = 5.5 \times 10^6$

Fig. 19 (concluded)

32

$$\frac{y}{\delta} = 1.09$$

$$\frac{y}{\delta} = 1.84$$

NOISE

31 μSEC

$X = 29$ IN., $M_e = 6.79$, $Re'_\infty = 4.60 \times 10^4$ CM^{-1},

$Re_x = 4.8 \times 10^6$ $Re'_e = 5.4 \times 10^4$ CM^{-1},

$R_\theta = 2290$, $u_e = 1225$ m/SEC, $\lambda = 0.0015$

FIGURE 20

APPEARANCE OF BURSTS, IN THIS INSTANCE WITH SURFACE BLOWING

33

CONDITIONS: Po = 350 PSI (Re$_L$ = 8.4 X 10^6)

λ = 0

α = 0

REGION SURVEYED

CRITICAL LAYER FOR LAMINAR INSTABILITIES

$Y/\delta = (1 - \frac{1}{Me})$

BOUNDARY LAYER EDGE (FROM MEAN FLOW MEASUREMENTS)

CONE SURFACE

X STATION (INCHES)

Y INCHES

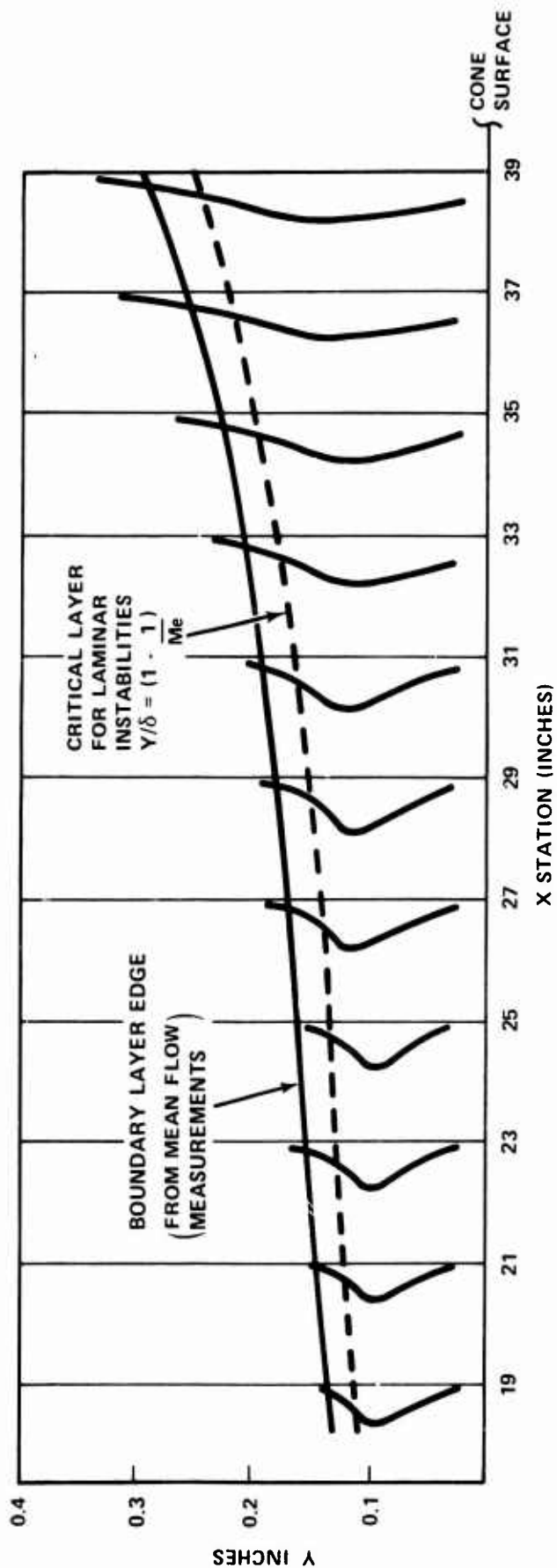0.4 0.3 0.2 0.1

19 21 23 25 27 29 31 33 35 37 39

FIGURE 21

LOW-RESOLUTION HOT-WIRE SIGNAL TRAVERSED ALONG y/δ = 0.7 AND AT x = 19,27,31 AND 39 INCHES FROM CONE TIP (FROM TOP)

34

FIGURE 22
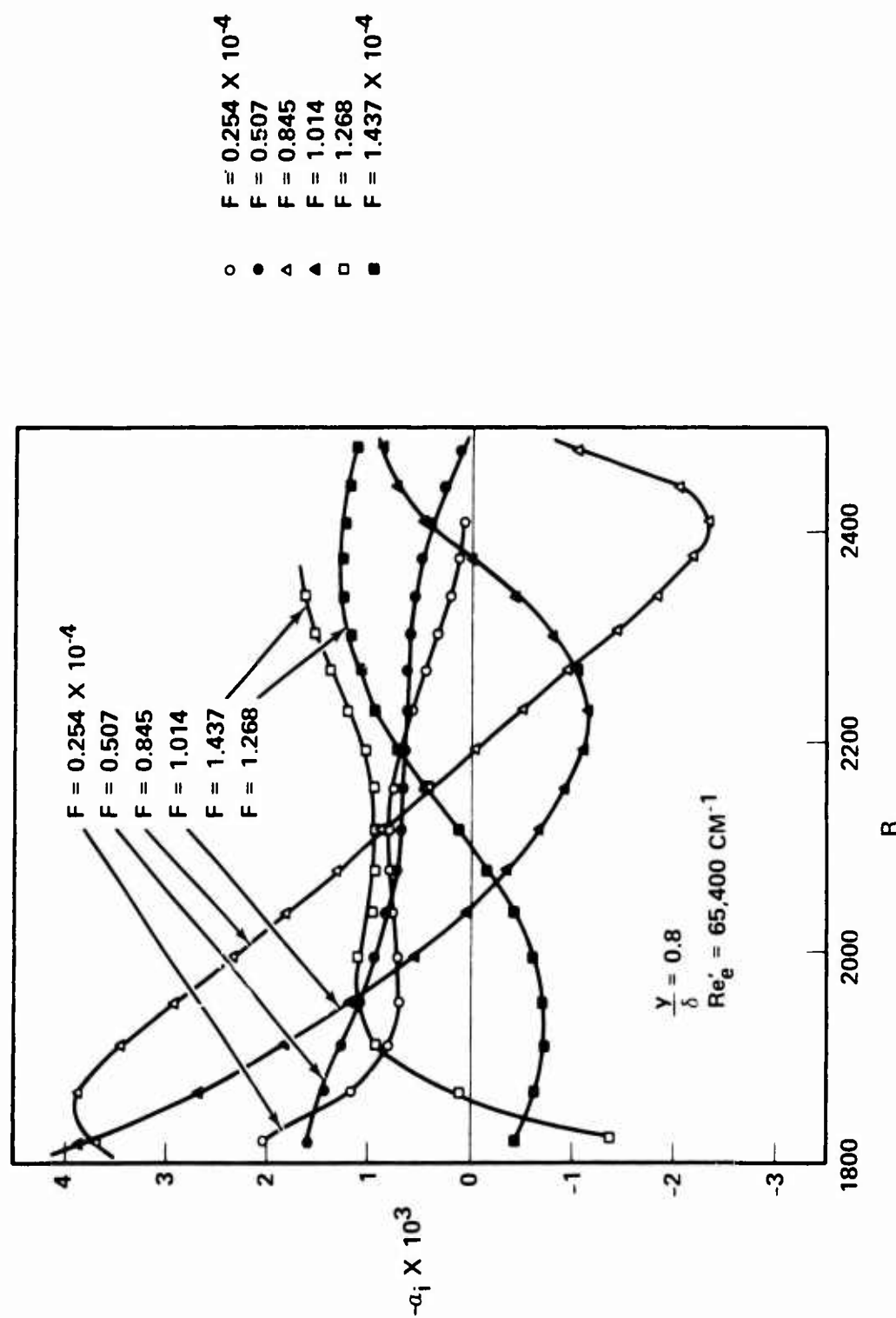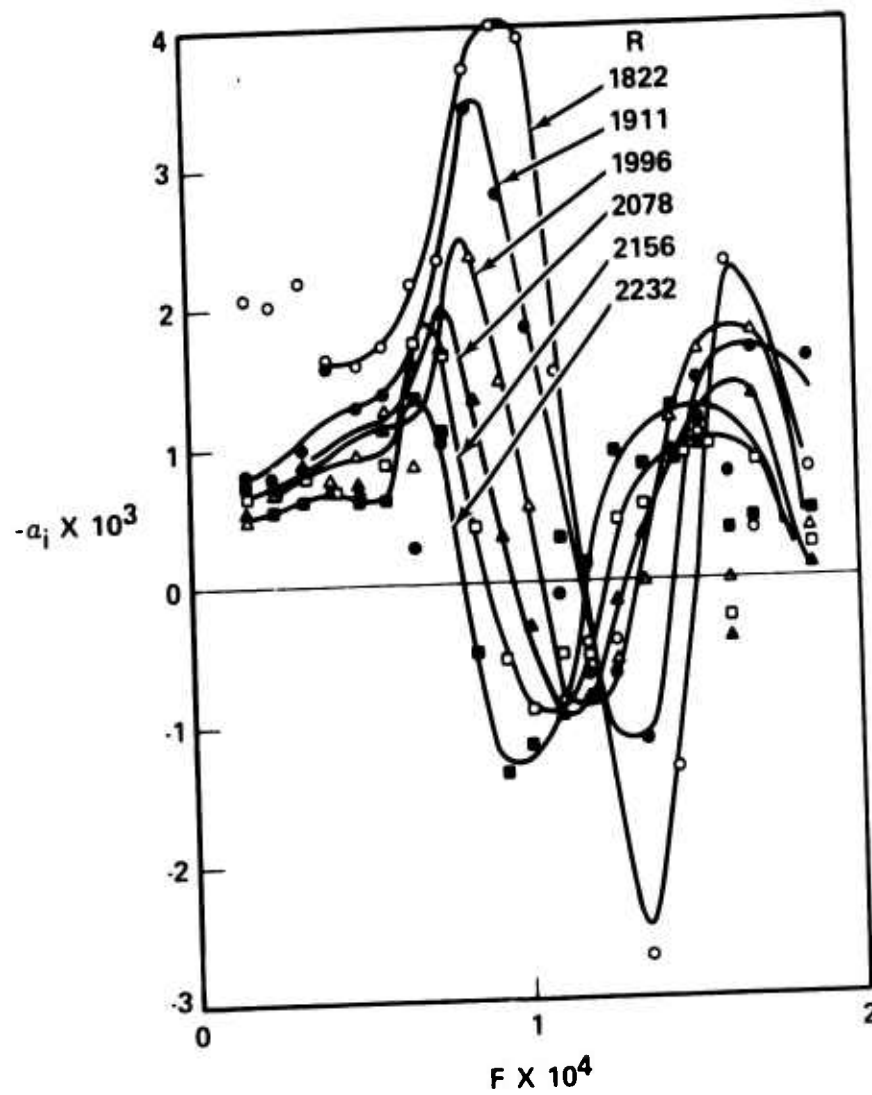
EVOLUTION OF AMPLIFICATION RATE ALONG CONE SURFACE

$F = 0.254 \times 10^{-4}$
$F = 0.507$
$F = 0.845$
$F = 1.014$
$F = 1.268$
$F = 1.437 \times 10^{-4}$

$\frac{y}{\delta} = 0.8$

$Re'_e = 65,400 \ CM^{-1}$

$-\alpha_i \times 10^3$

R

35

FIGURE 23

AMPLIFICATION SPECTRUM

36

PRESENT   KENDALL
DATA

$M_e = 7$ $M_e = 7.7$
$T_w/T_o = 0.78$ $T_w/T_o = 0.60$

NEUTRAL
BOUNDARY

2×10^{-4}

MAX LOCAL
AMPLIFICATION

THEORY,
2ND MODE ($\psi < 45^\circ$)
MAX LOCAL
AMPLIFICATION

$\dfrac{2\pi f}{u_e \, Re_e'} \equiv F$

10^{-4}

0

TRANSITION

DAMPED?

AMPLIFIED

AMPLIFIED

DAMPED

AMPLIFIED

DAMPED

AMPLIFIED

1400 1600 1800 2000 2200 2400 2600

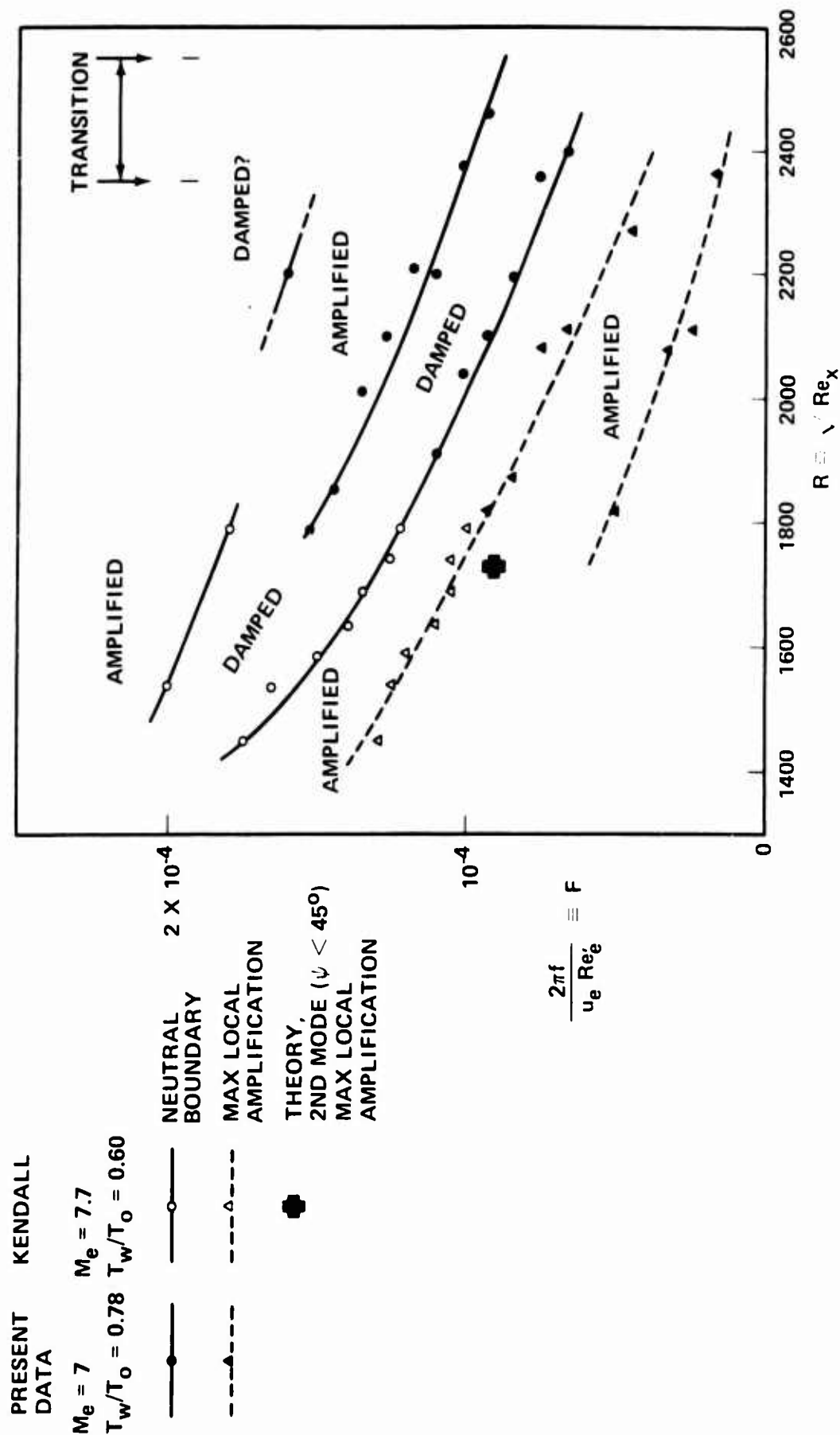$R\ \overline{z}_{\ \prime}\ Re_x$
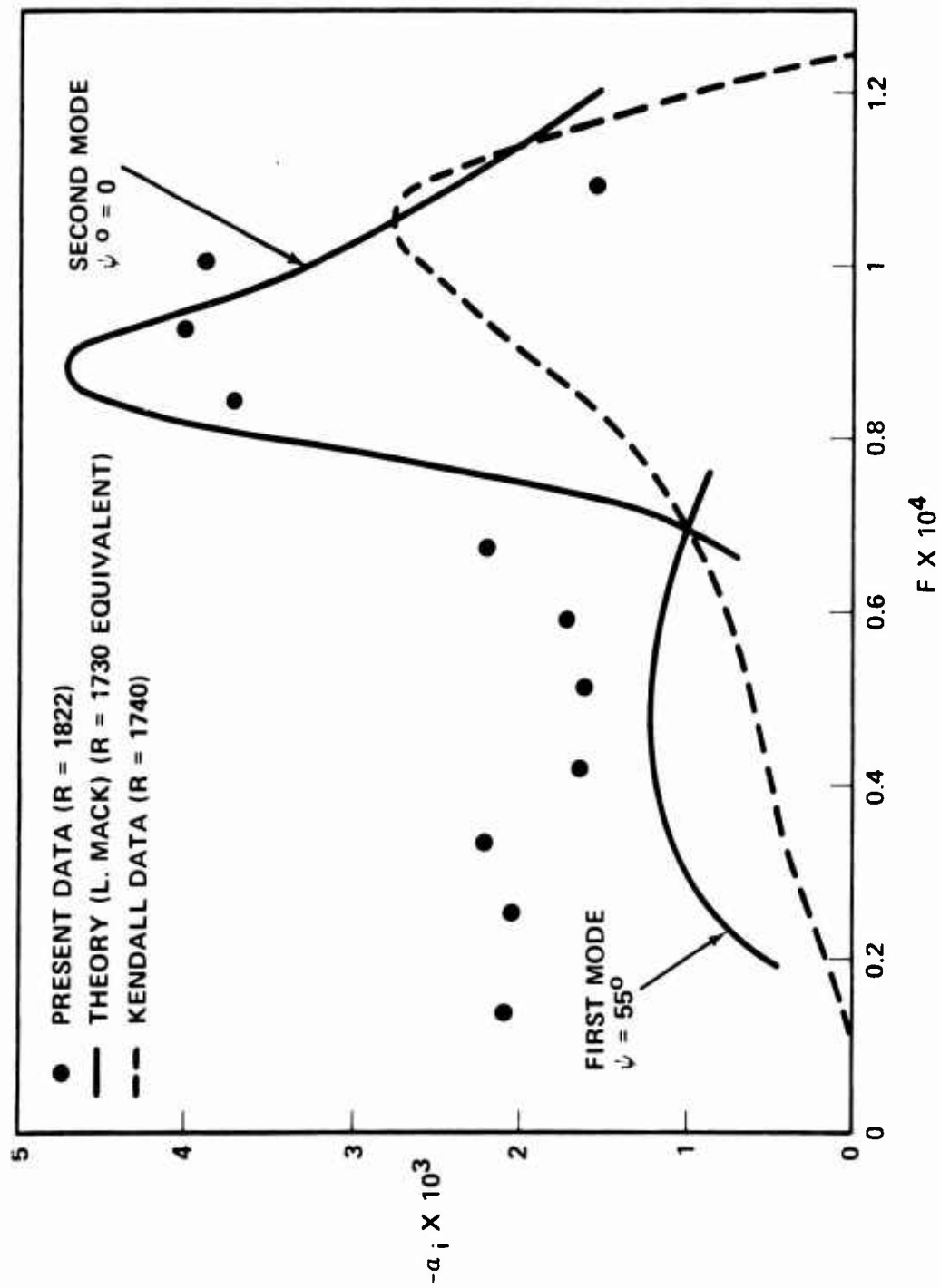
FIGURE 24

STABILITY DIAGRAM

37

FIGURE 25

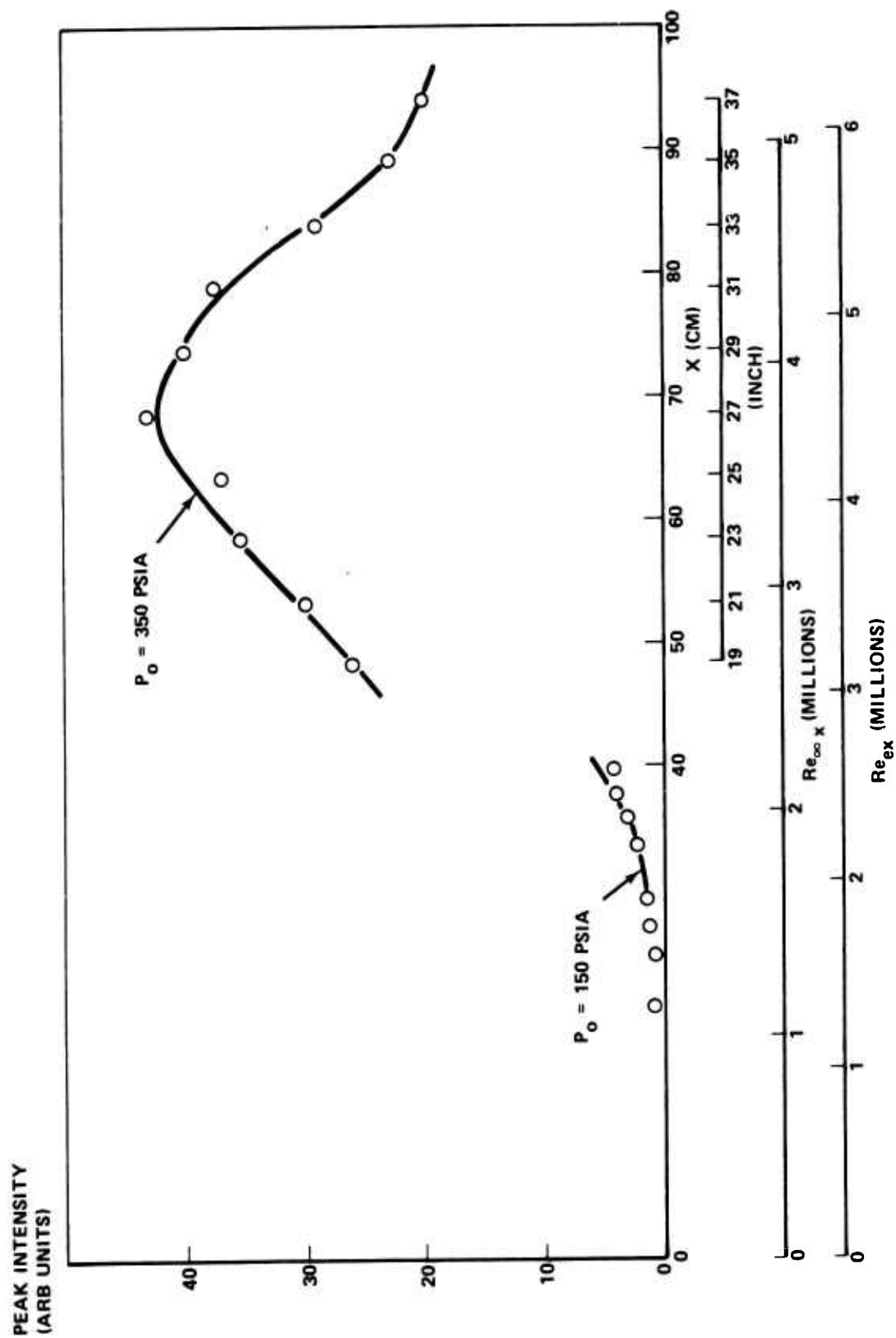COMPARISON OF EXPERIMENTAL STABILITY DATA WITH THEORY

FIGURE 26

VARIATION OF SPECTRAL PEAK INTENSITY OF THE LAMINAR WAVES